

# Fracture path in brittle thin sheets: a unifying review on tearing

**Benoît Roman**

**International Journal of Fracture**

ISSN 0376-9429

Volume 182

Number 2

Int J Fract (2013) 182:209-237

DOI 10.1007/s10704-013-9869-5



**Your article is protected by copyright and all rights are held exclusively by Springer Science +Business Media Dordrecht. This e-offprint is for personal use only and shall not be self-archived in electronic repositories. If you wish to self-archive your article, please use the accepted manuscript version for posting on your own website. You may further deposit the accepted manuscript version in any repository, provided it is only made publicly available 12 months after official publication or later and provided acknowledgement is given to the original source of publication and a link is inserted to the published article on Springer's website. The link must be accompanied by the following text: "The final publication is available at [link.springer.com](http://link.springer.com)".**

# Fracture path in brittle thin sheets: a unifying review on tearing

Benoît Roman

Received: 15 March 2013 / Accepted: 26 June 2013 / Published online: 24 July 2013  
© Springer Science+Business Media Dordrecht 2013

**Abstract** We review several studies of crack path in brittle thin sheets where large out of plane bending is involved. Fracture path are observed to be very reproducible. We present a unifying framework based on an energetic point of view. A simplified description, where the sheet is considered to behave as an inextensible fabric, captures important features of experiments: the fact that fracture path seems to obey geometry. We quantify the possible effects of additional bending and stretching terms, and estimate the validity of the model.

**Keywords** Plate mechanics · Crack path · Thin sheets

## 1 Introduction

We define “tearing” as the situation where fracture propagation in a thin plate is coupled to large out-of-plane displacements. These situations are common in everyday life (when opening a package [Monsalve and Gutierrez 2000](#) or removing wallpaper [Hamm et al. 2008](#)), and have implication in engineering design because slender structures are commonly used (for example the hull of a boat may be torn by a rock [Cerup-Simonsen et al. 2009](#)), but they are also responsible for

the formation of peculiar ice rafts ([Vella and Wettlaufer 2007](#)).

The classical picture of Linear Elastic Fracture Mechanics (LEFM) usually applies ([Bui 1978](#); [Lawn 1993](#); [Leblond 2003](#)) to a crack front propagating in a thick (or infinite) body. How do cracks propagate in thin structures such as brittle sheets, where fracture front may be reduced to a point propagating in a surface?

In this article we review recent academic studies on the quasistatic<sup>1</sup> tearing path in isotropic brittle plates, with the goal of organizing them in a unifying framework. A global remark is that the crack paths seem to be unusually reproducible. We will show how this surprising robustness of tearing paths is related to the central role of geometry in the mechanics of thin plates (basic facts on fracture and thin plates mechanics are reviewed in the remaining of this introduction). We explain this peculiar behavior by the remarkable geometrical simplicity of a newly formulated first order model (presented in Sect. 2), the *inextensible fabric model*, with consequences on tearing developed in Sect. 3. This first order model is unusual, because it includes the full geometrical non-linearities of the problem (which are essential to non-linear plate mechanics), but neglects the elasticity of the material. Finally we review attempts of a more complete treatment of the problem in Sect. 4.

---

B. Roman (✉)  
PMMH UMR 7636 CNRS/ESPCI/UPMC/Paris Diderot,  
ESPCI, 10 rue Vauquelin, 75005 Paris, France  
e-mail: benoit@pmmh.espci.fr

---

<sup>1</sup> See [Villermaux and Vandenberghe \(2013\)](#) for a review of recent studies on dynamic tearing of brittle thin sheets.

## 1.1 Crack path in three-dimensional fracture mechanics

Before turning to cracks path in thin sheets, it is interesting to present briefly the question of crack path selection in classical three-dimensional LEFM, where we can define stress intensity factors. Griffith's criterion states that a pre-existing crack propagates when it releases enough energy (work of the operator and stored elastic energy) to compensate for a cost of fracture  $G_c$  per area of the new surfaces.<sup>2</sup> In term of stress intensity factors, the energy release rate for propagation *in the direction of the initial crack* is (plane strain)

$$G = \frac{1 - \nu^2}{E} (K_I^2 + K_{II}^2) + \frac{1 + \nu}{E} K_{III}^2$$

If  $K_{II} = K_{III} = 0$ , fracture therefore propagate for a critical value  $K_I = K_{Ic}$ , where  $K_{Ic}$  is the fracture toughness of the material. The expression for  $G$  is also valid for a crack changing direction through a kink with a given angle, if the stress intensity factors  $K$ s are the one that the crack tip undergoes after it has turned and propagated an infinitesimal distance in the new direction (Amestoy and Leblond 1992).

The selection of the direction of propagation is still debated, and two criterions are proposed.

- In an isotropic material, the *Principle of Local Symmetry* (Cotterell and Rice 1980; Goldstein and Salganik 1974; Leblond 2003) assumes that a crack continues its straight path if the stress field is symmetric with respect to this direction. Looking at the linear elasticity solutions, we see that this is the case if  $K_{II} = 0$ . In a continuous experiment where the loading is varied continuously, one expects a crack to adapt smoothly its path so as to cancel mode II. If a condition  $K_{II} \neq 0$  is suddenly imposed, then it is thought that the crack will kink and choose a new propagation angle such that right after the kink, it will satisfy  $K_{II} = 0$ .
- Another point of view is to imagine that the magnitude of the loading is increased progressively, and to suppose that cracks propagate as soon as they can, in the direction which first satisfies Griffith's criterion. If the material is isotropic, cracks propagate in the direction  $\theta$  which *maximizes the energy*

*release rate*  $G(\theta)$  for a fixed loading (Bourdin et al. 2008).

These two criterions actually coincides if propagation is smooth: to say " $K_{II} = 0$ " is equivalent to say that " $G(\theta)$  is maximum in the initial direction of the crack" (Chambolle et al. 2009; Cotterell and Rice 1980; Amestoy and Leblond 1992).

But if the crack is loaded with a non zero  $K_{II}$ , it must abruptly changes direction in a kink. Starting from a loaded crack, the stress intensity factors experienced by a kinked extension can be computed (Amestoy and Leblond 1992), together with the energy release rate in different directions. It is found that the direction which maximizes the energy release rate does not satisfy  $K_{II} = 0$ . The two criteria disagree, and although the difference in angle between the two predicted directions is very small (and is almost indistinguishable in experiments) this leads to some uncomfortable issues.

We will adopt a pragmatic conclusion: as long as we are not interested in kinking points of the crack path, both criterion give the same result.

## 1.2 Tearing thin plates

We can think of a crack in a thin plate as a fracture front propagating in a 3-dimensional object, whose thickness  $t$  happens to be smaller than the other lengthscales (typical size  $L$ ). But traditional approach to thin plates mechanics takes advantage of the small parameter  $t/L$  to reduce elasticity in the direction of the thickness, and obtain 2dimensional description. In this point of view, the crack tip becomes a point and the crack path is a 2-dimensional curve.

### 1.2.1 Stress intensity factors in thin plates

A possible approach for the description of a crack singularity in a thin elastic plate is to define the equivalent of the stress intensity factors for linear thin plate elasticity equations. Williams found the singular solutions for Kirchhoff plate equations (Audoly and Pomeau 2010; Love 1944; Timoshenko and Woinowski-Krieger 1959) around the crack tip (Bui 1978; Williams 1961; Zehnder and Viz 2005). In addition to the usual in-plane modes  $K_I$  and  $K_{II}$ , there are two other modes,  $k_1$  and  $k_2$  which correspond to a symmetric bending mode

<sup>2</sup> However we should keep in mind that  $G_c$  is not a well defined material property, and may depend on the details of the plastic flow in the process zone: fracture toughness usually depends on the nature of the loading (mode mixity).

and antisymmetric twisting-transverse shearing mode.<sup>3</sup> The energy release rate for propagation (again in the direction of the crack) is [Zehnder and Viz \(2005\)](#)

$$G = \frac{1}{E}(K_I^2 + K_{II}^2) + \frac{\pi}{3E} \left( \frac{1+\nu}{3+\nu} \right) (k_1^2 + k_2^2)$$

Two difficulties arise if we were to follow this approach.

- First, we are actually interested in situations with large geometric non-linearities, and the validity of this approach (based on linear plate equations) is not easy ([Hui et al. 1998](#)), as well as the practical computation of the stress intensity factors from the imposed large scale loading.
- A second question is to deduce the direction of propagation from the values of the stress intensity factor. What is the equivalent of the Principle of Local Symmetry? The stress field associated with  $k_1$  is symmetric with respect to fracture direction, whereas that of  $k_2$  is antisymmetric (like usual mode II). But the angular dependence of these two antisymmetric mode is different. The condition for a symmetric stress field is  $k_2 = K_{II} = 0$ . Should we consider that these two conditions are necessary for a crack to propagate straight? But we only need *one* condition to determine an angle.

### 1.2.2 Variational approach

Because of these difficulties, we will adopt an energy point of view in the remaining of this article: Griffith's criterion and the criterion of maximum energy release rate. The energy release rate will be computed from variation of the elastic energy of the system (and operator's work), and not from an explicit calculation of the generalized stress intensity factors. This approach has the advantage of allowing large out-of-plane displacements if one can evaluate bending and stretching energies. It is not often possible to obtain exact expression for these energies, but we will present an interesting approximated simplified model (the inextensible fabric model) which captures some of the essential features of tearing paths.

This approach assumes that the process zone is small enough that the crack tip can be treated as a point (the

<sup>3</sup> Because of inherent assumption in the kinematics of Kirchhoff equations the shear stresses diverge like  $r^{-3/2}$  instead of  $r^{-1/2}$ , a feature which can be corrected within a Timoshenko–Reissner plate theory ([Bui 1978](#); [Zehnder and Viz 2005](#)). But these effects are only relevant at a distance to the tip inferior to the thickness.

details of the local field around it are not important). Another important assumption is that fracture energy  $G_c$  is independent of the fracture mode.

### 1.3 Mechanics of slender bodies: bending, stretching and geometry

For a comprehensive review of the mechanics of slender bodies, see [Audoly and Pomeau \(2010\)](#), [Timoshenko and Woinowski-Krieger \(1959\)](#), [Pogorelov \(1988\)](#), [Love \(1944\)](#), [Mansfield \(1989\)](#). Here we choose to introduce bending and stretching rigidity, and the role of geometrical non-linearities on a simple example. In this article we will consider only a linear elastic behavior of the material (small strains), but non-linearities due to large displacement (geometric non-linearities). In a thin sheet, the in-plane displacement is associated with in-plane stretching rigidity, whereas curvature of the surface leads to a restoring torque proportional to curvature (bending rigidity with a modulus  $B$ ).

*Linear behavior: Bending and Stretching.* Consider the simple example of a cantilever strip (thickness  $t$ , and width  $w \gg t$ ) clamped at one end, submitted on the other end to a force  $F$  small enough that the response is linear. If the force is applied along the axis of the beam, stresses  $\sigma = F/tw$  will lead to a displacement of the end of the beam by  $\delta_s = FL/twE$ , where  $E$  is Young's modulus of the material.

If now the load is applied perpendicularly to the beam, the applied torque  $M = FL$  leads to a curvature at the clamp  $\kappa = FL/B$ , where  $B = Et^3w/12(1-\nu^2)$  is the bending rigidity ([Audoly and Pomeau 2010](#); [Timoshenko and Woinowski-Krieger 1959](#); [Love 1944](#); [Landau and Lifshitz 1967](#); [Mansfield 1989](#)) and  $\nu$  is Poisson's ratio. This linear response between curvature and torque is valid as long as  $kt \ll 1$ . This leads to a typical deflection given by  $\kappa \sim \delta_B/L^2$ , so that  $\delta_B \sim FL^3/EI$ .

As a result, the ratio of displacement is  $\delta_s/\delta_B \sim (t/L)^2$ . For the same force, thin strips will undergo large out-of-plane deflection (and therefore stresses), but small change of length. This is a direct consequence of slenderness, independently of the material properties. It is therefore tempting to consider that rods and sheets are inextensible in the limit of vanishing thickness.

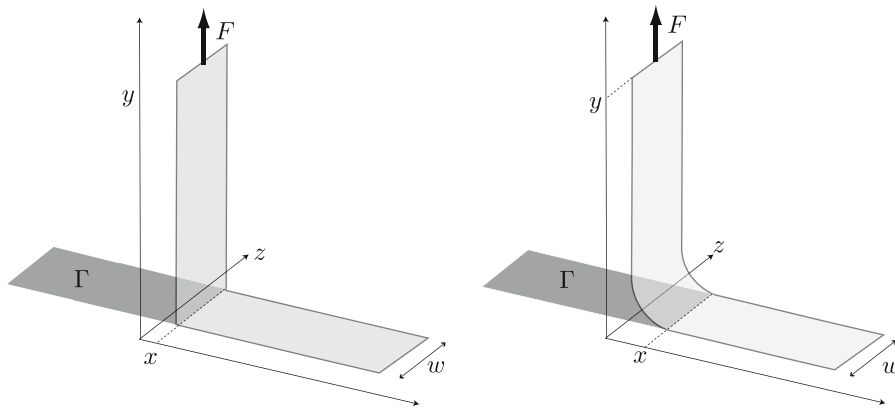


**Fig. 1** Peeling of an adhesive strip perpendicularly to the substrate. *left*: a strip with no bending rigidity, with a sharp corner at the peeling line. *Right*: a strip with finite bending rigidity. In

fact this second figure can be seen as a zoom of the figure on the left close to the peeling front

*Geometrical inextensibility.* But boundary conditions may prevent the existence of *isometric* solutions (shapes compatible with no extension of the neutral line or surface). In fact this is in general the case for a good design in engineering, because the rigidity of the structure is largest. For example the expected load on a truss should generate stretching of its members, not pure bending.<sup>4</sup>

In the case of sheets, the condition of isometric deformation is very restrictive. Surfaces isometric to a plane, called developable surfaces have zero Gaussian curvature everywhere (Struik 1988). They can be seen as a collection of straight lines with the supplementary conditions that the tangent plane is constant along each of these lines. If they are extended far enough, such surfaces always include singularities where the curvature is infinite. Particular examples are cylindrical surfaces (singularity at infinity) and conical surfaces (one singular point).

Crumple a piece of paper in your hands: isometric solution compatible with these boundary conditions will in general include singularities (Ben-Amar and Pomeau 1997; Witten 2007). These crumpling singularities are in practice regularized because they would lead to infinite bending energy (Audoly and Pomeau 2010; Pogorelov 1988; Witten 2007), at the cost of some localized stretching (Ben-Amar and Pomeau 1997; Lobkovsky et al. 1995).

<sup>4</sup> This argument defined the shape of Eiffel’s tower (Eiffel 1900) for a maximum rigidity against distributed wind loading.

We see that in the elasticity of thin sheets the interplay of two modes of deformation gives a non-trivial and rich behavior, where the role of geometry is very strong. Although considering slender bodies as inextensible is tempting (and we will use this model in this article), this approximation leads to some inconsistencies in some cases: boundary conditions may result in some in-plane strain (either diffuse or localized) for non-trivial geometrical reasons.

## 2 The “inextensible fabric” approximation applied to peeling

Before entering the subject of tearing, we present an approximation used in the measurement of adhesion energies (Kendall 1971, 1975). We will then use this approximation (that we name “inextensible fabric model”) for tearing configurations.

Consider a thin sheet adhering to a substrate (adhesion energy  $\Gamma$ ), with width  $w$ , bending rigidity  $B = Et^3/12(1 - \nu^2)$  due to a Young’s modulus  $E$  and thickness  $t$ , pulled perpendicularly to the substrate (see Fig. 1) with an imposed force  $F$ . All the material stuck on the substrate is in its rest state and has zero elastic energy.

The work of the operator is converted to elastic and surface energy (Griffith’s criterion for the propagation of interfacial fracture):

$$Fdy = dE_{el} + \Gamma w dx, \tag{1}$$

where  $E_{el}$  is the elastic energy of the flap, and is a function of the force  $F$ , the geometry (width  $w$  and length  $L$  of the flap) and material properties.

### 2.1 Inextensible plate, with zero bending rigidity: the inextensible fabric model

In this approximation (Fig. 1-left), the main point is that there is no elastic energy in the system and  $dE_{el} = 0$ . Geometry also imposes  $dy = dx$  because lengths are conserved (inextensibility). The propagation of a peeling front therefore requires a constant force (Kendall 1971)

$$F = \Gamma w.$$

### 2.2 Including stretching

We keep bending stiffness  $B = 0$  for now, but consider finite membrane rigidity. Because it is subject to a pulling force  $F$ , the flap is stretched, with a strain  $\epsilon = F/Etw$ . The elastic energy stored in the extensible flap  $E_{el} = EtwL\epsilon^2/2 = F^2L/(2Etw)$  increases with flap size  $L$ , and may therefore be large if the flap is long. We will however see that it is possible to ignore the stretching of the plate in most cases, even if the flap is extremely long.

In fact the peeling force  $F$  is here also constant (and so is the strain  $\epsilon$ ). Because the flap is elastic, Eq. (1) now includes a term  $dE_{el} = Etw\epsilon^2dL$ . Another difference with previous case is that the distances are stretched so that when the front advances,  $dx = dL = dy/(1 + \epsilon)$ . Finally Eq. (1) becomes

$$F \left( 1 + \frac{F}{2Etw} \right) = \Gamma w,$$

a result first shown by Kendall (1975). It is surprising that the peeling force  $F$  is found lower than if the flap were inextensible, because of the additional work needed for the ever increasing stretching energy. But in fact the extensibility of the strip leads to a larger travel distance for the same advance of the peeling front, so that the operator indeed provides a larger energy (than in the inextensible case) by the work of a lower force. Because we assumed  $F/Etw = \epsilon \ll 1$  for the use of linear elasticity, we simply find  $F \simeq \Gamma w(1 - \epsilon/2)$  at linear order. The conclusion is that the peeling force is

only slightly modified by the finite rigidity of the material if the flap is not seen to stretch by a large amount ( $\epsilon = F/Etw \ll 1$ ).

### 2.3 Bending energy in an inextensible strip

We now consider that the strip is inextensible (infinite in-plane rigidity) but has a non-zero flexural rigidity. The shape and elastic energy of the flap is invariant in the  $z$  direction, and can therefore be determined using an inextensible *elastica* equation. The solution of this problem can be written analytically (see Appendix 6.1 with  $\phi = \pi/2$ ):

$$E_{el} = (2 - \sqrt{2})\sqrt{FBw},$$

under the assumption that  $L \gg \sqrt{Bw/F}$ , or in other terms, that the size of the fold (boundary layer where curvature is localized) is much smaller than the length  $L$  of the flap.

In this framework, the solution of Griffith's criterion involves a constant force  $F$ . Indeed, with constant  $F$  and  $w$ , the fold shape remains identical. As a result  $dE_{el} = 0$  and  $dy = dx$ , so that Eq. (1) leads again to

$$F = \Gamma w.$$

When the bending rigidity of the sheet  $B$  goes to zero, the elastic energy of the flap  $E_{el} \sim \sqrt{B}\Gamma w$  does vanish, as well as the radius of curvature (and the size) of the fold<sup>5</sup>  $R \sim \sqrt{B/\Gamma}$ . At the end we are left with a straight fold shape having sharp angle on the peeling line, and zero bending energy. This inextensible model with finite bending rigidity converges towards the inextensible, infinitely flexible sheet limit, or the "inextensible fabric model".

### 2.4 Conclusion

We have seen in this simple situation that the "inextensible fabric" approximation does a good job at predicting peeling forces and elastic state of the system under certain conditions:

As we could have expected, stretching of the material can be neglected if strains  $\epsilon \sim F/Etw \ll 1$  are

<sup>5</sup> We find again the elasto-capillary lengthscale (Bico et al. 2004; Roman and Bico 2010) over which surface and bending energies equilibrate.

small. We see that stretching energy  $F^2L/2Et w$  vanishes when rigidity  $Et$  becomes infinite, as we can expect for a spring with increasing rigidity  $k$  under a constant force (the energy  $F^2/2k$  decreases with rigidity).

The situation is reversed with bending energy: it becomes negligible when bending rigidity vanishes in this strongly non-linear regime. Indeed for low bending rigidity, the geometry of the system is only modified in a boundary layer with size  $R \sim \sqrt{Bw/F}$ , where curvature (on the order of  $1/R$ ) and bending energy are localized. The total bending energy in this system  $\sqrt{BFw}$  does vanish with rigidity  $B$  (the loading  $F$  kept constant). The infinitely bendable approximation describes well the geometry if the size of system  $L \gg \sqrt{Bw/F}$  is large compared to the size of the fold.

We observe that for a given geometry and material, there is a range of force  $F$

$$Bw/L^2 \ll F \ll Et w. \tag{2}$$

for which the strip is close to being inextensible, infinitely bendable, and therefore can be assumed to store no elastic energy. This regime exists when  $Bw/L^2 \ll Et w$ , which is equivalent to  $t \ll L$ , or when the sheet is very thin. A rigorous demonstration of this fact<sup>6</sup> can be found in Marigo and Meunier (2006).

### 3 Inextensible fabric model: fracture mechanics obeys geometry

In this section we study how fracture propagates in an inextensible fabric (i.e. a plate with zero bending modulus  $B$ , but infinite in-plane rigidity). We will see that this leads to a simple model for crack propagation, where geometry plays the dominant role. We will also compare its predictions to experiments in the different configurations described in the literature, which we classify according to the number of cracks involved and the type of loading (“pulling” or “pushing”).

An important assumption will be that the number of crack remains constant in the experiment (it is very difficult to initiate new cracks in the material used in experiments). In all this section, the argument will be developed with imposed force  $F$ .

<sup>6</sup> As the slenderness ratio  $e = t/L$  vanishes, 3D-elasticity converges towards the inextensible, infinitely bendable model if the normalized loading  $\eta = F/Et w$  follows  $\eta \sim e$ . This falls in the conditions (2), which can be rewritten into  $1 \gg \eta \gg e^2$ .

### 3.1 Two cracks configurations (pulling and pushing are straight)

#### 3.1.1 Pulling on the flap

We consider the case where a flap between two notches is pulled in a fixed direction  $\phi$ , as in Fig. 2. In the assumption of inextensible fabric, if the plate is clamped on the dashed boundaries, only the flap can be moved out of its initial position, the rest of the sheet being rigidly linked to fixed boundaries. Indeed any displacement of other material points would generate an elongation prohibited by inextensibility. This also true if the sheet is not clamped on its boundaries, but instead adheres on a flat substrate from which it is pulled. In this case a straight peeling front joining the cracks propagates simultaneously with them. We note  $\Gamma$  the adhesion energy ( $\Gamma = 0$  corresponds to clamped boundary conditions) and  $w$  the width of the fold.

No elastic energy is involved in this inextensible fabric approximation: as the crack propagates, energy conservation (Griffith’s criterion) is simply:

$$F du = \Gamma w dl + 2G_c t ds$$

Suppose that fracture propagates in direction given by  $\theta$  in Fig. 2. The geometric conditions  $du = dl(1 - \cos \phi)$  and  $dl = ds \cos \theta$  (see Fig. 2), lead to the following expression for the energy release rate per crack

$$G(F, \theta) = \frac{F(1 - \cos \phi) - \Gamma w}{2t} \cos \theta. \tag{3}$$

The geometrical factor  $(1 - \cos \phi)$  is well known in the theory of peeling (Kendall 1971), but applies equally to the clamped boundaries situation (with no adhesion energy  $\Gamma = 0$ ).

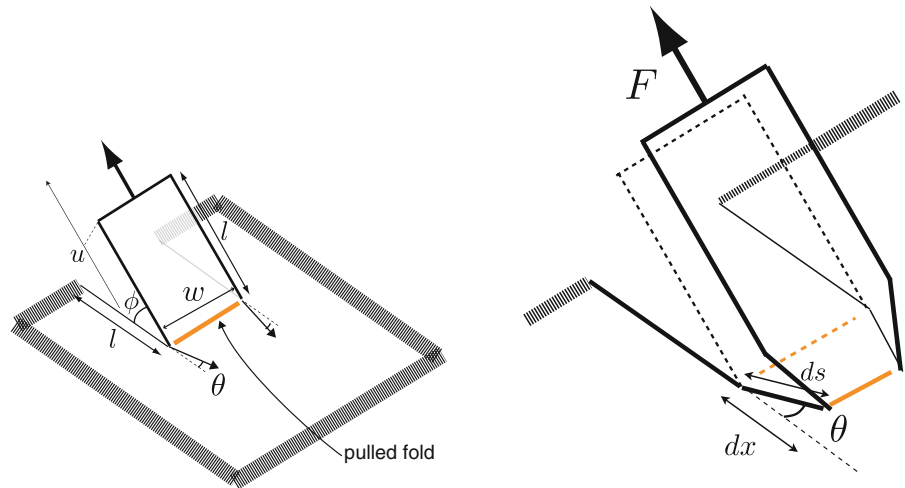
The consequence is that in all these configurations, the energy release rate for a fixed loading  $F$  is maximum for  $\theta = 0$ , and we obtain the first rule:

**Cracks propagate perpendicularly to a pulled fold.**

(4)

The force necessary for crack (and peeling) propagation depends on material properties  $F = (\Gamma w + 2G_c t)/(1 - \cos \phi)$ . However we note that the direction of propagation is independent of all material properties (fracture energy  $G_c$ , material rigidity and thickness  $t$ , magnitude of adhesion  $\Gamma$ ), and independent of many loading characteristics: the size of the flap  $w$ , the location of clamped boundary conditions, the angle of

**Fig. 2** Pulling on two cracks. The sheet is clamped on the dashed boundaries, with two notches. The resulting flap is pulled in a direction with an angle  $\phi$  with respect to the plane. What is the direction  $\theta$  of propagation?



pulling  $\phi$ , and the speed of the experiment (as long as kinetic energy can be neglected)!

In experiments (Hamm et al. 2008) the crack path are indeed remarkably reproducible, however the cracks are observed to converge ( $\theta > 0$ ) and we will see in Sect. 4.1 how this convergence is related to the finite bending rigidity of the sheet.

Recent experiments have shown how these laws are modified when a flap is torn from a sheet adhering on a curved cylindrical substrate (Kruglova et al. 2011). The geometry of the flap is obtained through a reflection with respect to a plane  $P$ , an operation that conserves lengths (see Fig. 3a). The fold joining the two cracks is therefore lying along the intersection of this plane with the curved substrate, a portion of an ellipse, which geometry is set in the experiment by the curvature of the substrate and the pulling angle  $\phi$ . Unless the peeling angle is  $\phi = \pi$ , this means that the fold is a curved line in the plane of the sheet. For simplicity we will consider the case with  $\phi = \pi/2$ , so that  $u = l$ , and Griffith's criterion simply reads  $Fdl = \Gamma wdl + 2G_c t ds$ . The energy release rate  $2tG = (F - \Gamma w)ds/dl$  is maximum when the ratio  $ds/dl$  is maximized, or in other words, when the cracks advance the least amount for a given step  $dl$  of the front.

The smallest path length for the crack to reach the displaced (but identical) front is obtained when propagation is perpendicular to the front (as illustrated in Fig. 3c). We therefore find that rule (4) still holds, if understood locally. This is a consequence of the fact that cracks are point singularities in this model: each

crack propagates perpendicularly to the local orientation of the fold in its neighborhood, and we expect the rule (4) to be general.

In the case of curved substrate the two cracks will therefore not keep a constant distance, but will converge, or diverge<sup>7</sup> depending on the sign of the curvature of the cylinder. In the case of Fig. 3, the cracks are diverging.

### 3.1.2 Pushing on the flap

We now consider the case of a blunt object pushing between two notches, as in Fig. 4. The sheet is clamped on all the dashed boundary conditions. Part of the sheet bends out of the way, until the objects hits the boundary of this bendable zone, which we will call the "active front". We note that the bendable zone covers the exact same geometrical area as the flap in previous configuration, for the same geometrical reasons, so that the "active front" and the "pulled fold" share the same geometrical line.

Because there is no easy experimental realization of a peeling version of this pushing configuration (where the plate would not be clamped on the boundaries, but adheres on a substrate), we only consider the clamped configuration and take  $\Gamma = 0$ .

<sup>7</sup> The experimental flap shapes are more complex because converging effects due to finite bending rigidity (Sect. 4.1) has to be considered, and may dominate over the diverging terms for weak substrate curvature, strong adhesion, or thick sheets (Kruglova et al. 2011).

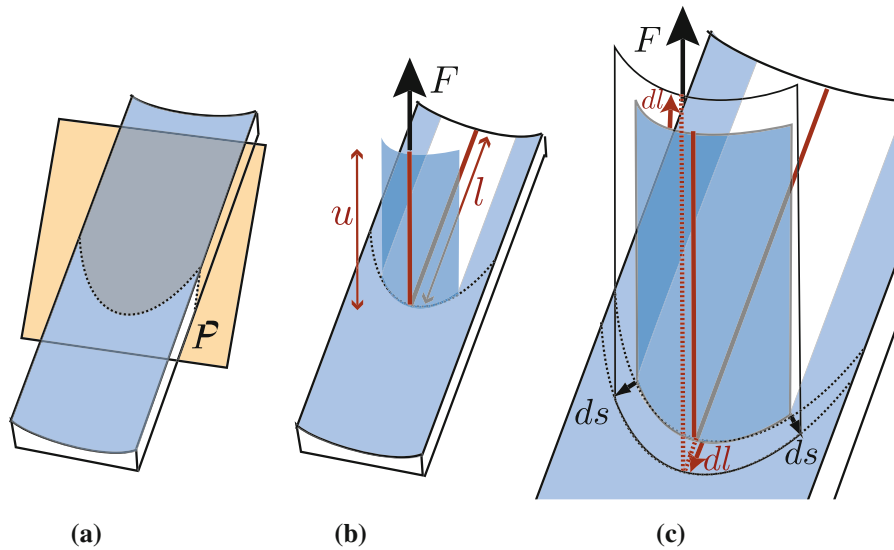


**Fig. 3** **a** Inextensibility requires that the peeling front from a cylindrical substrate lies at the intersection (*dotted line*) of the substrate with a plane *P* (*yellow*), an ellipse. **b** Indeed, the complete geometry of the peeling flap is obtained by reflection with respect to plane *P*. The height above the substrate *l* is equal to the length *u* for a perpendicular peeling angle  $\phi = \pi/2$ . **c** When

the cracks propagate symmetrically by *ds*, the front will lie on the same ellipse, but displaced by *dl*. The ratio *dl/ds* is therefore maximized when the cracks propagate perpendicularly to the peeling front, leading to a diverging propagation in the situation presented here

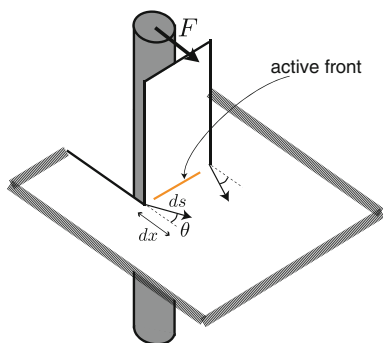


**Fig. 4** Pushing on two cracks. The sheet is clamped on the dashed boundaries, with two notches. The resulting flap is pushed upon by a blunt object. What is the direction  $\theta$  of propagation?

Here the energy release rate is again given by the rate of work of the operator,  $2Gtds = Fdx$ , with the simple relation  $ds \cos \theta = dx$ , so that we are lead to the same equation as (3) where  $\phi = \pi/2$ .

$$G(F, \theta) = \frac{F}{2t} \cos \theta$$

The maximum energy release rate therefore also predicts that in the pushing configuration  $\theta = 0$ , so that the fracture propagates in the direction perpendicular

to the pushed front, which is also here the direction of pushing. These two directions do not always coincide, and we will see in paragraph 3.3.1 (see in particular Fig. 11) that the general rule is

**Cracks propagate perpendicularly to a pushed front.** (5)

In experiments, small negative propagation angle  $\theta < 0$  are observed and cracks slowly separate. This can be attributed to in-plane strains (see Sect. 4.2.3).

### 3.1.3 Robustness of tearing path

We see that within this approximation the energy release rate *does not depend on material properties, nor on the history of the crack, nor on the actual size of the flap or location of clamped boundary conditions, nor speed of the experiment* (loading speeds are much lower than sound speed), but only on the direction  $\theta$  of the crack with respect to the fold/front, and intensity of the force. This is at the root of the remarkable reproducibility and robustness of the tearing crack paths that will be presented in the next sections.

We have also shown the rationale behind the organization of this review: there is a strong analogy between pushing and pulling in the inextensible fabric model, although the two situations sometimes lead to different behaviour in experiments because of thin sheet elasticity.

In fact if a pushing experiment is performed as in Fig. 4, an instability takes place (unexplained to our knowledge), and one of the crack wins over the other one which stops propagating. Pushing on two cracks is not generally observed (unless the material is plastically deformed (Tallinen and Mahadevan 2011; Wierzbicki et al. 1998)) and leads to single crack configurations, which are reviewed in the next section.

### 3.2 Pulling on a single crack (hyperbolae and spirals)

We review here several tearing experiments where only one crack propagates, and compare the trajectory of the cut with predictions by the inextensible fabric model.

#### 3.2.1 Trouser test

The “trouser test” is a standard configuration used to measure the fracture energy in thin plates and elastomers. In a strip with a cut, the two flaps are clamped and pulled away from each other (see Fig. 5). Here the work of the operator is  $Fdy$ , when the crack advances by a surface  $tds$ , with geometry imposing  $dy = 2ds \cos \theta$ . The energy release rate  $G = 2(F/t) \cos \theta$  is maximum for  $\theta = 0$ . The propagation is predicted in the direction parallel to the boundaries of the strip. In fact if the notch separates the strip in two flaps with equal width, the crack path should be straight ( $\theta = 0$ ) for reasons of symmetry, independently of the assumption of inextensible fabric. This straight propagation is observed in experiments where the flaps are pulled (Takei et al. 2013) or rolled on parallel

**Fig. 5** Trouser test geometry. We note  $\theta$  the angle of propagation

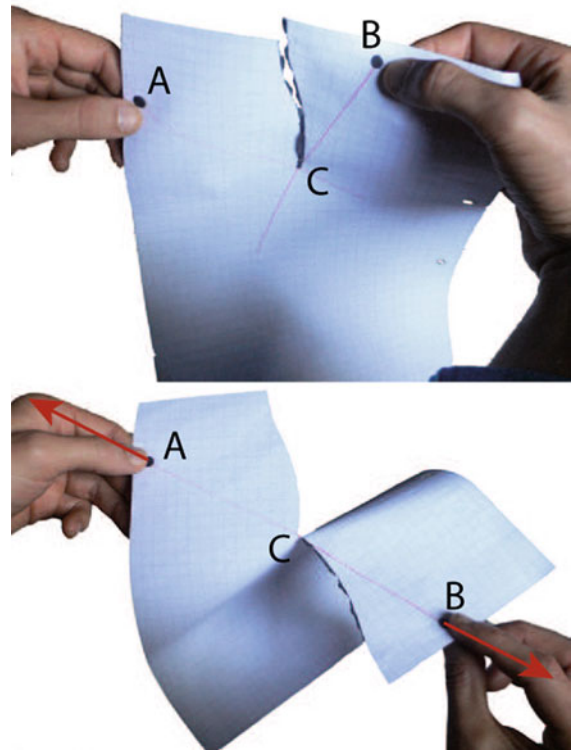
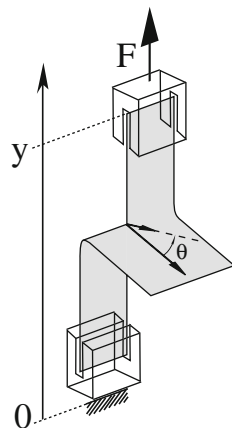


**Fig. 6** Two points on a flat sheet (left) are pulled away from each other (right)

cylinders (Bayart et al. 2010), even if the notch is off centered.

#### 3.2.2 Pulling on two points

An ingenious tearing experiment which somehow generalizes the trouser test configuration is reported in O’keefe (1994). A notch is cut in a thin sheet, and two points A,B are selected, one on each side of the notch. These two points are pulled away from each other, so that only forces (no torque) are applied, (see Fig. 6). In what direction does the crack propagate?

A key observation is that for infinitely bendable sheets, the two red lines (AC, BC) drawn on the sheet that join the pulling points to the crack tip C become a single straight line when loading is applied. This is a consequence of the fact that an infinitely bendable sheet cannot sustain torques. We note  $l$  the total distance between ACB in the loaded configuration. As the crack advances by a distance  $ds$ , the energy release rate is here  $Fdl$

Because the sheet is inextensible,  $l$  can also be found on the flattened sheet (initial configuration) by adding distances  $l_1 = AB$  to  $l_2 = BC$  measured along the red lines (Fig. 7). Simple geometry shows that  $dl_1 = \cos \theta_1 ds$  if

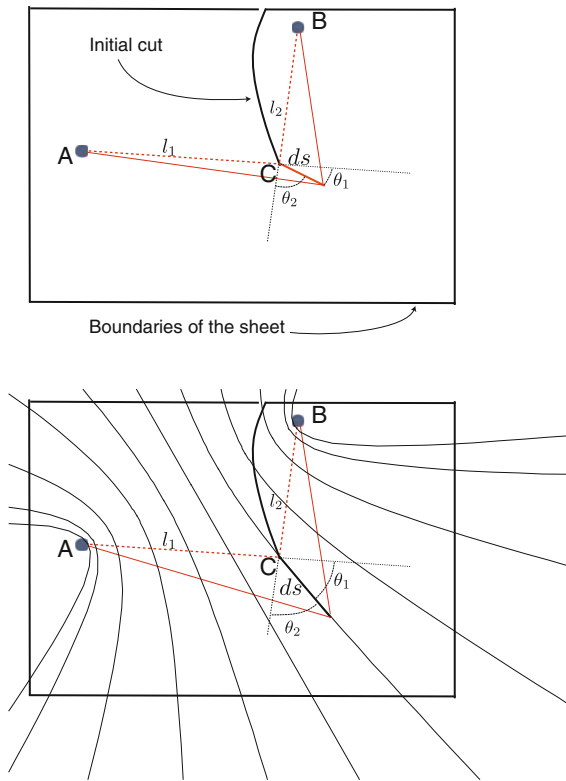


**Fig. 7** Tearing hyperbolae: the crack in C propagates when the sheet is pulled by points A and B. The optimal direction bisects the angles ACB ( $\theta_1 = \theta_2$ ). So that the possible trajectories are hyperbolae, with focal points in A and B, drawn on the right

$\theta_1$  is the angle between the direction of the crack and the line AC. As a result, the energy release rate becomes  $Fdl/t ds = F(\cos \theta_1 + \cos \theta_2)/t$ . Because the sum  $\theta_1 + \theta_2$  is constant, the maximum energy release rate is achieved when  $\theta_1 = \theta_2$ : the crack propagates in the direction that bisects the sector ACB.

As a result, the crack path has the property of being at each point C tangent to the bisector of angle ACB. This is the definition of a hyperbola with focal points A and B. All the hyperbola have an asymptote. Indeed when the crack moves away from A and B,  $l_1 \sim l_2 \gg AB$ , so that the crack almost follows the line (AC) which is the same as (BC), with a constant angle with respect to the segment AB. In this asymptotic case we recover the trouser-test symmetric geometry. Depending on the initial position of A,B and the crack tip C, one of the hyperbola (and final asymptote) is selected. If in the initial case  $l_1 < l_2$ , the crack path turns initially towards A. If  $l_1 = l_2$ , then this property stays true all along the crack path which follows a straight line.

Some experiments were performed with paper in O'keefe (1994) to check this theory, but the agreement

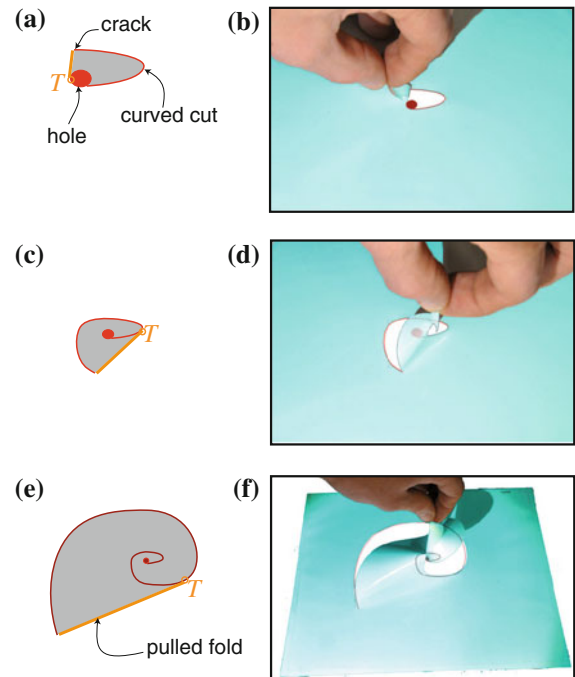


**Fig. 8** Cutting a brittle sheet along a line leads to a propagation in a spiraling shape. **a** The initial seed (a hole plus a curved line) and **b** the resulting flap. **c–d** The crack propagates perpendicularly to the fold. **e–f** The crack path evolves into a spiral. Gray region corresponds to the convex hull of the crack path. In dotted blue line is the pulled fold

with the theory was obtained with an ad hoc fitting parameter introduced to account for anisotropy of the paper (see Takei et al. 2013 for a study of anisotropy in tearing).

### 3.2.3 Pulling on a flap, with one crack

We now come back to situations where we pull on a flap, but this time with only one crack. We start with a sheet held on its boundaries (or adhering on a flat substrate), that is cut along a particular path: a circle plus a curved line (as in Fig. 8a). This defines a flap (Fig. 8b) that can be pulled perpendicularly to the plane of the sheet. The crack should therefore propagate perpendicularly to the pulled fold, as we have seen before. But as the crack propagates, the geometry of the flap evolves in a more complex way: the fold rotates progressively (Fig. 8d), so that the crack tip follows a spiraling trajectory (Romero et al. 2013) (Fig. 8f).

Spiral patterns are sometimes observed in the fracture of strained film bonded to a substrate: converging spirals are reported in drying layer (Argon 1959; Dillard et al. 1994; Leung et al. 2001; Néda et al. 2002; Xiaa

and Hutchinson 2000) when the material debonds from the substrate. Diverging fracturing spirals are sometimes observed (Lebental 2007; Meyer et al. 2004; Sendova and Willi 2003; Wan et al. 2009) in similar systems, where stresses are due to the film deposition process. However in both cases the spirals seem to be archimedean, with the radius decreasing or increasing by a specific characteristic distance at each turn. Fracture propagation is due to residual tensile stresses, so that the loading is also completely different from the tearing situation studied here.

Following the inextensible fabric model, the evolution of the fold can be deduced from simple geometry. We first look for the points which stay fixed in an inextensible sheet with clamped boundaries when a given continuous line is cut. All the points of a segment joining two fixed points are fixed: they cannot be displaced in any direction without changing the length of the segment. But this argument does not hold if the segment intersects the crack trajectory because the material segment is not continuous. The area swept by all segments joining two points of the boundary without intersecting the cut line is therefore the region which is rigidly fixed. The remaining points are not rigidly linked to the boundary,<sup>8</sup> and are free to move out-of plane. This is the flap region, which can also be defined as the set of segments joining any two points of the cut line, *i.e.* the convex hull of the cut line.

For example on Fig. 8, the flap corresponds to the convex hull of the previous cut (in grey on drawings on the left). The advancing front of this convex hull is the pulled fold (orange line), a segment which starts on the advancing crack tip, and ends tangentially to the cut line at point  $T$  (drawn in orange).

Consider the height  $z$  of the 3D structure on Fig. 9 obtained when the operator pulls upward on the tip of the flap. Because the sheet is considered infinitely flexible,  $z$  is simply the distance between the pulling point and the line along which the flap is fixed (the advancing front, also denoted pulled fold, in orange) measured along the cut flap: this is the length of the shortest curve drawn along the flap that links the tip to the front (in red on Fig. 9). The distance  $z$  is therefore the length of the path from the pulling point to point  $T$ . Under loading by the operator, this curved line becomes straight, causing the complex three-dimensional structure bent around it (at no energetic cost in this model).

Because inextensible fabric have no elasticity, the energy release rate reduces to the work of the operator  $G = Fdz/ds$ . The direction of propagation therefore maximizes the geometrical ratio  $dz/ds$ . This is the direction which minimizes the crack advances  $ds$  for a fixed  $dz$ .

<sup>8</sup> Things are more complex if there are several non-connected cuts.

If the height increases by  $dz$ , this leads to an advance by  $dz$  of point  $T$  along previously cracked trajectory (Fig. 9-right). The position of the pulled fold (orange line) is set, because of the tangency condition. The crack tip must lie on this line, and the minimal distance from previous position is obtained through a jump perpendicular to this fold line.

As a result, the crack propagates perpendicularly to the pulled fold: here again, we have recovered the rule (4). In fact, this is not too surprising because the local loading configuration near the the crack tip (one side pulled up, the other side attached to the boundaries) is identical to that experienced in a double crack geometry (as in Fig. 2).

We now have a construction rule for the the crack trajectory, starting from a seed line: the crack always propagates perpendicularly to pulled fold (boundary of the convex hull of the crack path), which always stays tangent to previous crack trajectory. We note that this construction rule is based on angles, has no internal length scales, so that it applies equally at all scales. A famous geometric curve with this scale-independent shape property is the logarithmic spiral, whose radius grows exponentially with the number of turn. It is sometimes called equi-angular spiral, because angular properties are conserved along the spiral. Indeed, the geometry of the spiral at one point is identical to that around any other point, only scaled out and rotated. Amongst those spirals, only one has the pitch that corresponds to the construction rule that we defined: its radius grows like  $\exp(p\psi)$  ( $\psi$  being the polar coordinate angle), where  $p \sim 0.274$  (Romero 2010; Romero et al. 2013).

Starting from any geometry of initial seed, we do observe on a simple numerical integration that the construction leads to a spiral trajectory, which asymptotes towards this spiral. In the experiments (Romero 2010; Romero et al. 2013), we observe a behavior compatible with an exponential growth, but with a slightly different exponent (see Sect. 4.2.2), and with oscillations which we interpret as anisotropy effects.

An interesting feature is the robustness of this natural spiral path (independent of position of boundaries, speed, pulling angle), and its exponential growth. It may be used as an easy opening trick for packages. As the user pulls on the pre-cut tab, the crack spirals and quickly reaches the boundaries of the package. An entire face of the package is destroyed, and the product may be removed easily (easy opening patent Cerda et al. 2012).

### 3.3 Pushing on a single crack (oscillations and spirals)

In recent years, several quasistatic tearing experiments have involved the propagation of a single crack by pushing a blunt tool through a thin sheet.

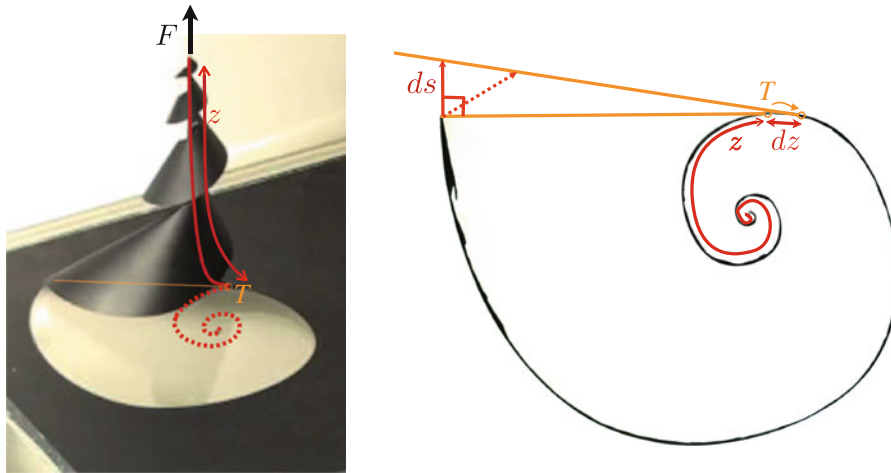


**Fig. 9** Pulling on a flap with only one crack leads to a spiral. (left) The pulling fold is along a straight segment (in orange) joining the crack tip to a point  $T$  where it is tangent to the crack path. The height of the tip of the flap above the clamped plane  $z$  is given by the length of the crack path from the flap tip to the

tangency point  $T$ . (right) During fracture, the tangency point  $T$  advances by  $dz$ , so that the crack must lie on the new tangency line. The maximum energy release rate corresponds to the direction of shortest step  $ds$  for the crack to reach the new orange line: perpendicular to the fold line

### 3.3.1 Oscillation

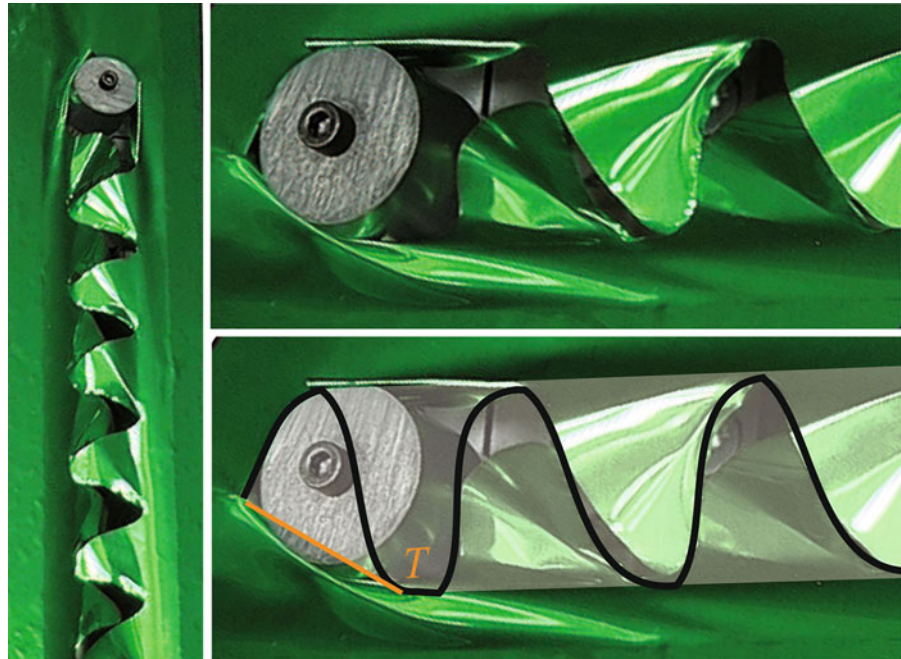
In a typical experiment (Atkins 2007; Audoly et al. 2005; Ghatak and Mahadevan 2003; Reis et al. 2008; Roman et al. 2003; Tallinen and Mahadevan 2011), a blunt tool perpendicular to the plane of the sheet is displaced with a constant velocity along a straight trajectory. The sheet is clamped on its boundaries and includes a single notch in which the tool is inserted. If we use a sharp tool, like a knife, the material is cut at the tip of the tool and the crack path follows the trajectory of the tool. But if the tool is blunt, the crack path quickly takes a regularly oscillating path (see Fig. 10). We note  $w$  the maximum width section of the tool measured perpendicular to the pushing direction, as can be seen on Fig. 13.

These oscillating shapes are reminiscent of the oscillating crack path observed in thermal loading (Adda-Bedia and Amar 1996; Ronsin et al. 1995; Yang and Ravichandar 2001; Yuse and Sano 1993) when a hot glass strip is dipped in cold water. If the dipping speed is high enough that thermal diffusion does not have time to operate, thermal stresses develop and the plate fractures. Depending on the speed, a straight crack path may become unstable and an oscillating path develops. But the mechanism is clearly very different from the tearing configurations in this review. A more similar phenomenon is observed in the wake of a cylinder in a layer of visco-elastic fluid (Gladden and Belmonte 2007) which may behave like an oscillating fracture.

Experiments Audoly et al. (2005), Ghatak and Mahadevan (2003), Reis et al. (2008), Roman et al. (2003) have revealed striking features of this phenomenon: the crack path is independent of the speed of the tool (as long as it stays much smaller than the typical dynamic fracture speed), it is independent on the geometry of the clamping conditions (which may be close or far away from the tool path). The amplitude and wavelength are observed to be proportional to the width of the tool, on a large range of scale. The amplitude to wavelength ratio depends weakly on the shape of the object. These observations break down when the tool width becomes comparable to the thickness of the sheet: for thin enough tools, the oscillations disappear through a discontinuous transition (Roman et al. 2003), or even in the case of relatively large width to thickness ratio when the tool is strongly inclined (Reis et al. 2008).

The inextensible fabric model gives some interesting predictions for this phenomenon. We first define the convex hull of the crack path, which can be seen as the reunion of “flaps” (Figs. 10, 11) and is again the zone where out-of-plane displacements of the plate are possible. The blunt tool must therefore always entirely lie in this area. When the object touches (and pushes) the convex hull boundary front, the crack must therefore propagate so that the convex hull extends and still includes the tool. It is easier to consider the rather artificial situation in Fig. 11 where the object is drawn small compared to the amplitude of the oscillations. The boundary of the convex hull is a line

**Fig. 10** Oscillatory crack path: the wake in a solid. Although the out-of-plane bending is complex, the crack path is very regular. Notice the flaps in the wake of the cylinder



(drawn in yellow) that joins the crack tip to the point  $T$  of tangency. Suppose that the tool is pushed out of the convex hull by a distance  $dz$  as in Fig. 11, leading to a crack advance by  $ds$ . Griffith criterion also writes  $Fdz = G_c t ds$ , where  $F$  is the force imposed by the operator. The direction for the maximum energy release rate<sup>9</sup> is again the one that maximizes  $dz/ds$ . We can repeat the argument seen with Fig. 9: the minimal crack advance  $ds$  compatible with a given advance of the tool by  $dz$  takes place in direction perpendicular to the convex hull front. Note that the direction of propagation is *independent of the direction of pushing, and of the actual place where the object pushes on the active front*.

We have recovered the propagation rule (5): cracks propagate perpendicular to a pushed front.

When the crack propagates, simple geometry sets the new convex hull and therefore the evolution of the active front. Numerical integration<sup>10</sup> of these geometric rules quickly converges towards a periodic oscillating trajectory

<sup>9</sup> An argument based on the same principle was developed in Atkins (2007) for the case of a cylindrical rigid tool. With the additional assumption that the crack tip was assumed to be located on a circle centered on the tip but with larger radius. Because no elastic energy was attributed to the sheet, the ratio  $dz/ds$  was minimized to obtain the angular velocity of the crack, and therefore the crack path.

<sup>10</sup> Interactive software written by B. Audoly, Institut Jean Le Rond d'Alembert, CNRS/UPMC, 2003.

(Fig. 12). The oscillation is divided in alternating symmetric phases: when the crack goes to the left, this is because the object, advancing straight, pushes leftward on a front (Fig. 12a, d, e). This phase stops when the pushing front is no more touched by the left side of the object, that is when the crack has reached a distance equal to  $w/2$  from the centerline (Fig. 12a, e). At this point the process should stop, but the object may now push on the other front (the right front) and a new phase may start, mirror symmetric from the previous one. We see that the oscillation path is a way for a single crack to do the job of the two cracks in Fig 4: open in an inextensible sheet a convex hull channel wide enough to always enclose the pushing object. Because the propagation rule (5) is independent of the size of the front, the crack path for a geometrically similar larger object should simply be identical but scaled up from the cut obtained with a smaller object.

More than that, if only the width  $w$  of an object is known, the crack path can be constructed as the curve which periodically repeats itself when the following geometrical rule is applied: propagate the crack perpendicularly to the convex-hull front line which is then advanced accordingly, and stop when a distance  $w/2$  from the centerline is reached. The process is periodic if the obtained curve is the mirror of the first one. The consequence of this simple argument is that the fracture wake in a thin sheet is *independent of the shape of the object* (and only depends on its width).

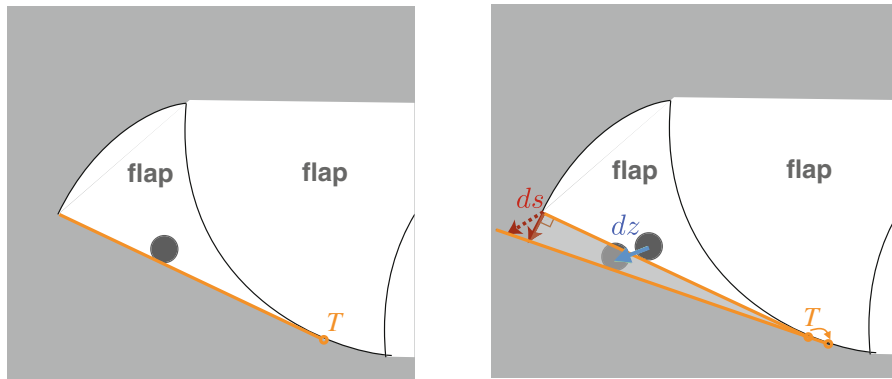
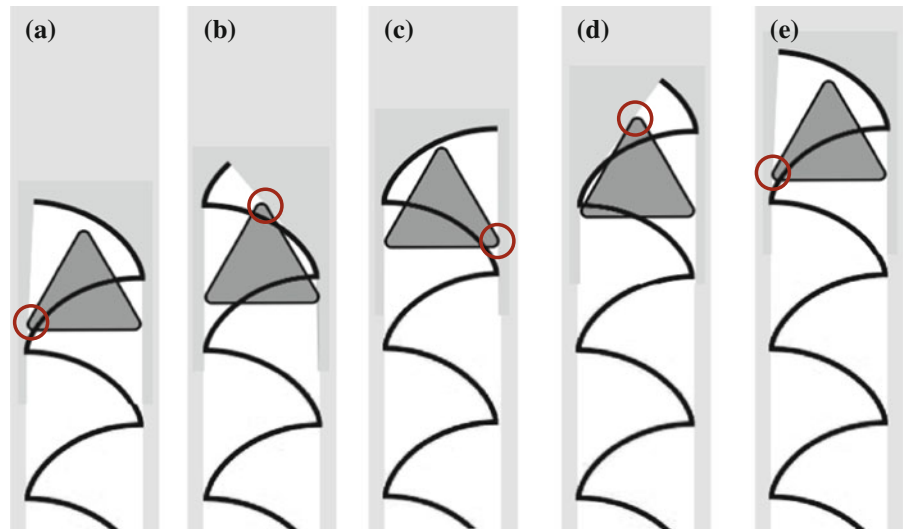


**Fig. 11** (left) The crack path convex hull defines “flaps” (white area) which easily bend around the tool. If the tool were to advance by  $dz$  and cross the boundary of the convex hull (in orange), it would generate stretching in the inextensible film. Instead the crack tip will propagate (right) by a distance  $ds$  so

that the pushed front (orange boundary) advances and the tool still belongs to the flap region (white). The direction of propagation for the crack that minimize  $ds/dz$  is perpendicular to the pushed front

**Fig. 12** Numerical evolution of geometrical rules for a triangle tool. In white, the convex hull of the crack path, and grey, the points rigidly linked to the clamped boundaries. The triangle always lies in the white area, and is in contact with a boundary at a point circled in red in cases **a**, **d**, **e**: during this “left” phase, the crack propagates towards the left. Soon after **a**, the triangle does not contact the left front, but hits the cut boundary, so that the mirror “right” phase takes place in **b**, **c**



This is shown in Fig. 13, where an experimental path for a disk tool is compared to that obtained from numerics with different tool shapes. In the numerics, even if the object is not left-right symmetric, the crack path will be the same and the wavelength is  $\lambda \sim 1.32w$ . Contrary to ad hoc assumption in Ghatak and Mahadevan (2003) there is no reason to believe that this shape is composed of arches of cycloids.

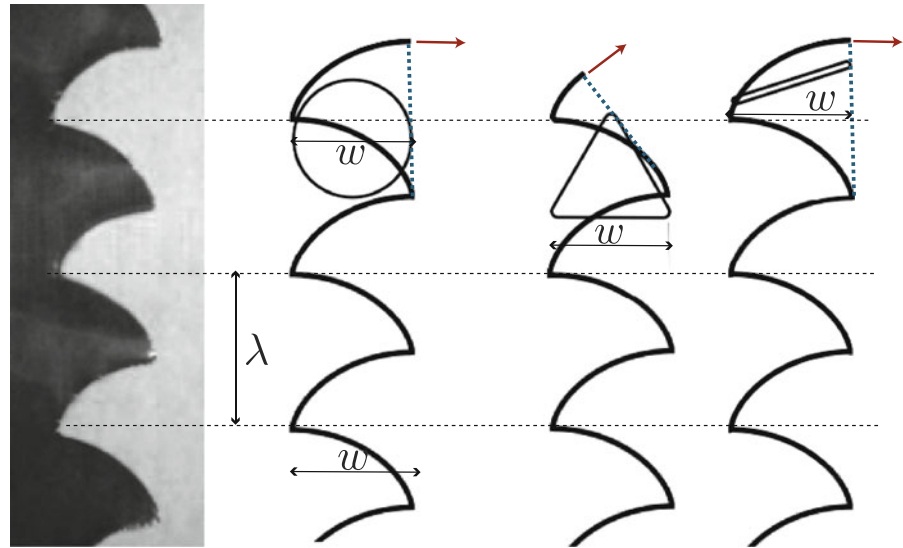
In experiments (Audoly et al. 2005; Roman et al. 2003), we observed that as long as the object is much larger than the thickness of the plate, the amplitude is comparable to the width of the object (between 0.75 and 0.95  $w$ ) for  $w$  varying from 0.3 to 50 mm, and wavelength to width ratio is found to vary between  $1.15 < \lambda/w < 1.5$  for very

different tool shapes and even for asymmetric shapes. The origin of these small variations are discussed in Sect. 4.2.4.

Although this argument gives an elegant explanation for the remarkable robustness of the crack path, it should be used with some care because of a hidden assumption: that the object always pushes on the active boundary of the convex hull. This assumption is not satisfied in two situations.

First, we used the implicit assumption that the left-right phases alternate after the active pushing front has become parallel to the pushing direction. In other words we assumed that the crack has reached one of the boundary  $x = \pm w/2$  before the foremost point of the object hits the convex hull limit. But this is only true if the blunt tool is

**Fig. 13** Oscillatory crack path: the wake in a solid. *Left to right*: picture of a sheet cut by a cylinder (disk). Simulation of geometrical rules for a similar cylinder, a triangle and an inclined plate. In dotted blue line is the active pushed front, always perpendicular to the crack path tangent. All the crack are pictured in a “right” phase, propagating towards the right, with the tool pushing towards the left of the pushing front



not too elongated along the pushing direction, for example for square or circle geometry (Audoly et al. 2005). In the opposite case, the crack path may start the mirror phase before the end of the previous one, and an interesting dynamics takes place: in general we observe several oscillations on a short wavelength / short amplitude around the object tip. But this does not open a wide enough channel for the tool, so that eventually a large scale (comparable to  $w$ ) phase takes place again. This phenomenon repeats in a complex but periodic crack path, see Fig. 14a. This peculiar behaviour is also qualitatively observed in our experiments (but was not reported in the literature).

A second, more frequent situation where our assumption always fails (even for non elongated tools) are the kink points where the system switches from one phase to the other. We have indeed assumed that the object always pushes on the active boundary of the convex hull. But in the case of a tool with disk geometry, we see that the object hits the convex hull on a curved cut line, not on a straight boundary originating on the crack tip (Fig. 14b). As a result, a small advance of the crack will not produce movement of the object, and therefore extracts no work. Without energy released, the crack cannot propagate, and if the crack cannot propagate in an inextensible fabric, the tool cannot advance, so that the system is locked. Propagation is possible only after the crack is allowed to jump for a finite distance, so that the pushing tool now touches the new convex hull active front. Within the inextensible fabric model, the system would therefore not allow propagation after one phase of the oscillation, even for infinite pushing force. In practice a dynamic jump of the crack is observed (see Sect. 4.2.4).

### 3.3.2 Pushing spiral

The oscillating path alternates left and right phases because the tool pushes alternatively on the left or right active front. It is possible to stay in one of these phases (Romero 2010; Romero et al. 2013), if the tool is continuously pushed against one of the active front, as described in Fig. 15: In the experiment, the tool is pushed against the front, which turns as the crack tip propagates. The movement of the tool has to be adjusted so that it continually pushes against the flat portion of the ridge. There are however many tool trajectories (consisting of pushing at different distance from the crack tip), but they all lead to almost identical crack path (Romero 2010). A spiraling path develops (Fig. 15), and within the inextensible fabric approximation, the spiral is identical to the self-developing pulled logarithmic spiral described previously (in experiments the observed pitches are however slightly different Romero et al. 2013).

### 3.4 Conclusion on inextensible fabric model

Assuming that the sheet behaves as an inextensible fabric, the direction of propagation for a crack maximizes the extraction of the operator's work. In a variety of examples which can be divided into pulling (on a flap) or pushing (with a blunt tool) configurations, we have seen that the angular distribution of energy release rate can be simply computed from geometry arguments.

The crack path is therefore independent of the speed of the experiment (as long as kinetic energy is not important),

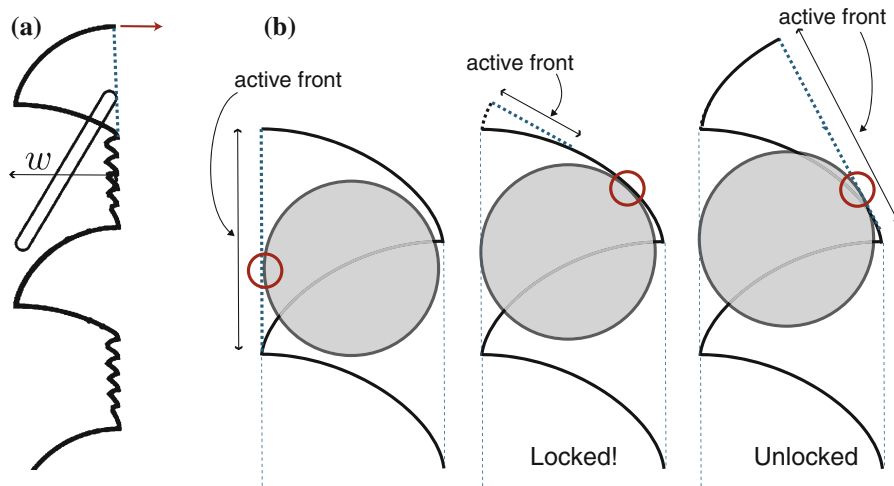
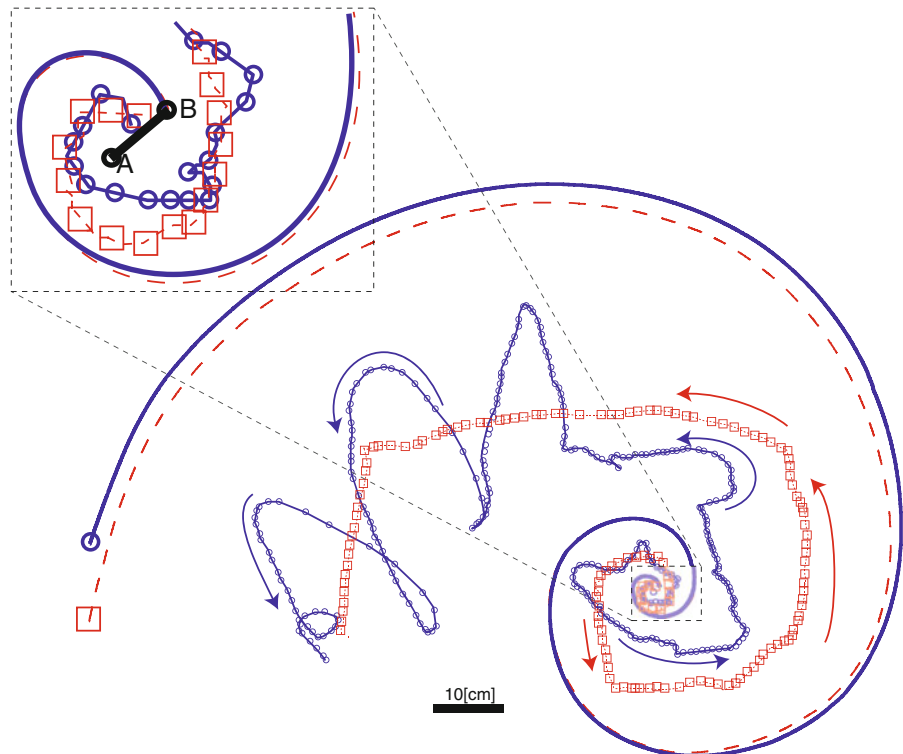


**Fig. 14** The universal shape model should not hold: **a** for an elongated the tool (like this inclined plate—numerical simulation), complex oscillations may arise. **b** At the kinking point, the left phase (figure on left) locks. In the center figure, a vanishingly small advance of the crack does not allow any advance of

the tool. This is because the tool does not push (red circle) on the active front (blue dotted line), but on the crack path. Only a large advance of the crack allows movement (figure on the right). Within this model, the system is geometrically locked. In practice a dynamic jump of the crack is observed

**Fig. 15** Two spiraling cracks obtained by the same initial conditions (continuous and dotted lines), and pushing always on the same active front of the convex hull with a blunt tool (Romero 2010; Romero et al. 2013). In circles and squares are represented the positions of the tool in the experiments at fixed time intervals corresponding to the crack path with the same color. Although the speed and trajectory of the tools are different, the crack path are close, as predicted by the zero thickness model



independent of the material properties and thickness of the sheet, independent of the location of boundary conditions. All these properties are unusual for a fracture

problem. The crack path is completely determined by geometrical rules and it seems that mechanics reduces to geometry.

These properties of the inextensible fabric model seem to explain the striking reproducibility of crack path in experiments. In the following section we study how these results are modified when thin plate elasticity is included.

#### 4 Including bending and stretching rigidity

Although the inextensible fabric model gives many interesting predictions on the crack paths in quasistatic tearing, we have seen that it misses some features (locking of the oscillating crack path, for example).

We would also like to estimate the error on the crack path when this approximation is used, and quantify the validity of the model when applied to experiments.

Because the mechanics of thin sheet is non-linear, the analysis is difficult and we will restrict the study to one case where an analytical solution can be found (pulling on a sheet with adhesion) and review simple estimates for other cases.

##### 4.1 A complete tearing solution: pulling on strongly adhering sheet

We start with the case of tearing a sheet adhering strongly on a flat substrate, because the elastic energy of the system can be computed exactly (Hamm et al. 2008). The shape is indeed almost invariant along the direction of the fold: if adhesion dominates ( $\Gamma w \gg G_c t$ ), the system is very close to the case of pure peeling, and we will use the results of appendix 6.1, which summarizes exact results on the peeling of an elastic beam.

The argument can be made equally with imposed force or imposed displacement. It is instructive to choose this time an imposed displacement  $u = \delta - l \cos \phi$ , which corresponds to peeling with an angle  $\phi$  (see Fig. 16 for definitions). When the length of the flap is large compared to the typical curvature of the fold, the elastic energy is a function  $E_{el}(w, l - \delta)$  of the width of the flap  $w$  and of the geometrical distance  $l - \delta$  which encodes the curvature of the fold.

$$E_{el}(w, l - \delta) = \frac{4Bw}{(l - \delta)} [1 - \cos(\phi/2)]^2$$

Although this expression is valid for a rectangular flap, we will use it for flaps with arbitrary shape where we take  $w$  as the distance between the cracks: the bending energy is localized in a small region (the fold), so that we can consider that the distance between cracks alone defines completely the elastic energy (see Appendix 6.2 for a justification). This is in fact an important property which explains why the crack path is here independent of

its past trajectory, in contrast with fracture front in a linear three-dimensional medium.

In absence of work of the operator (the displacement  $u$  is fixed), Griffith's criterion

$$dE_{el} + 2G_c t ds + \Gamma w dl = 0$$

is rewritten in  $G = G_c$  with the energy release rate per crack  $G$  given by

$$2Gt = -\frac{dE_{el}}{ds} - \Gamma w \frac{dl}{ds}.$$

We can compute

$$dE_{el} = \frac{\partial E_{el}}{\partial(l - \delta)} \Big|_w d(l - \delta) + dw \frac{\partial E_{el}}{\partial w} \Big|_{(l - \delta)}$$

where the notation  $\partial./\partial x|_y$  stands for a derivative with respect to  $x$  holding  $y$  fixed. Geometry imposes  $dl = ds \cos \theta$ ;  $d\delta = dl \cos \phi$ ;  $dw = -2ds \sin \theta$ , so that Griffith's criterion is

$$G(u, \theta) = \frac{\cos \theta}{2t} \left[ -\Gamma w - \frac{\partial E_{el}}{\partial(l - \delta)} \Big|_w (1 - \cos \phi) \right] + \frac{\sin \theta}{t} \frac{\partial E_{el}}{\partial w} \Big|_{(l - \delta)} = G_c \tag{6}$$

The direction of propagation is given by the equivalent characterizations:

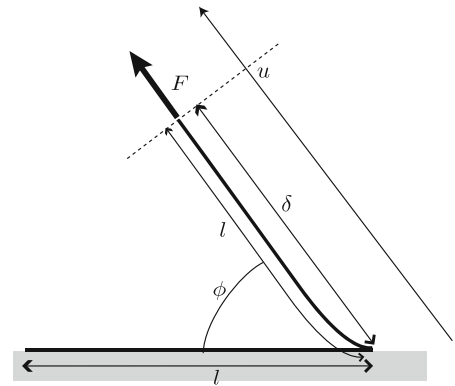
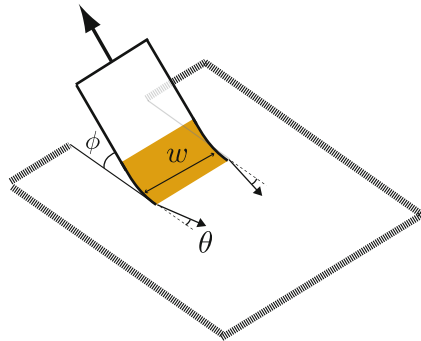
- the direction  $\theta$  that minimizes the displacement  $u$  necessary to satisfy propagation in that direction ( $G(u, \theta) = G_c$ ).
- the direction  $\theta$  that maximizes  $G(u, \theta)$  for a fixed displacement  $u$ . This formulation is easy to write, but we also have to impose in a second step  $G(u, \theta) = G_c$ .

We therefore obtain a second equation  $\partial G / \partial \theta = 0$  where all geometric distances  $w, l, u$  (and therefore also  $\delta$ ) are held constant in the computation of the angular derivative:

$$2t \frac{\partial G(\theta)}{\partial \theta} \Big|_{l, w, \delta} = -\sin \theta \left[ -\Gamma w - \frac{\partial E_{el}}{\partial(l - \delta)} \Big|_w (1 - \cos \phi) \right] + 2 \cos \theta \frac{\partial E_{el}}{\partial w} \Big|_{(l - \delta)} = 0 \tag{7}$$

It is useful to use an expression for the derivative at fixed  $w$ ,  $\partial E_{el} / \partial(l - \delta) = -E_{el} / (l - \delta) = -F$  (see Appendix 6.1), and finally the energy release per unit advance of the crack, and its angular derivative are

**Fig. 16** Tearing and peeling at imposed displacement  $u = \delta - l \cos \phi$



$$G(\theta) = \frac{F(1 - \cos \phi) - \Gamma w}{2t} \cos \theta + \frac{1}{t} \sin \theta \left( \frac{\partial E_{el}}{\partial w} \right)_{(l-\delta)} = G_c \tag{8}$$

$$\frac{\partial G(\theta)}{\partial \theta} = -\frac{F(1 - \cos \phi) - \Gamma w}{2t} \sin \theta + \frac{1}{t} \cos \theta \left( \frac{\partial E_{el}}{\partial w} \right)_{(l-\delta)} = 0 \tag{9}$$

If we inject  $E_{el} = 0$ , only the first terms remain, and we recover equation (3) of the inextensible fabric model. Note that in this fixed displacement argument, these “geometric” terms come from some derivatives of the elastic energy, which remains identical even when the elastic energy vanishes. If we were to use directly the inextensible fabric model and  $E_{el} = 0$  from the start in Eq. (6), the “fixed displacement” approach would fail. We always have to use an “imposed force” approach (as done in Sect. 3) with such an inextensible model, where these same terms are computed simply from the work of the operator.

We now have an extra elastic term due to the variation of elastic energy with the width of the fold  $w$ . We have two equations, with two unknowns: the force  $F$  (or equivalently the displacement  $u$ ) which determines the energy and the orientation  $\theta$  of the crack.

These equations are coupled but they can be gathered graphically in a vectorial balance (Fig. 17), which may be interpreted as an Eshelby force balance (Hakim and Karma 2009): equations (8) and (9) correspond to vectorial projection along axis  $(A, B)$  on Fig. 17. A projection of this balance along the horizontal and vertical directions  $(a, b)$  gives the more convenient expressions

$$F(1 - \cos \phi) - \Gamma w = 2G_c t \cos \theta \tag{10}$$

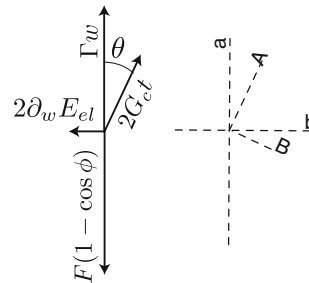


**Fig. 17** Equations for Griffith criterion (8) and the maximum energy release rate (9), can be represented in the form of a force balance which bears similarity with Young’s law for the wetting angle of a liquid

$$\left( \frac{\partial E_{el}}{\partial w} \right)_{(l-\delta)} = G_c t \sin \theta \tag{11}$$

Because  $\Gamma w \gg G_c t$  (strong adhesion), the first equation gives  $F(1 - \cos \phi) \simeq \Gamma w$ , whereas the second one gives  $\sin \theta \simeq 2\sqrt{FB/w}[1 - \cos(\phi/2)]/(G_c t)$

because the derivative  $\partial E_{el}/\partial w = E_{el}/w = 2\sqrt{FB/w}$ , as seen in appendix 6.1. We can inject the value of  $F$  and find

$$\sin \theta = \frac{\sqrt{2\Gamma B}}{G_c t} f(\phi) \quad \text{with} \quad f(\phi) = \left[ \frac{1 - \cos(\phi/2)}{\sin(\phi/2)} \right] \tag{12}$$

To our knowledge this equation has never been explicitated for all values of peeling angle  $\phi$ . We see that the tears are always converging ( $\theta > 0$ ), with an angle independent of the width  $w$ . The shape of the flap is therefore a triangle. This is in good quantitative agreement with experiments (Hamm et al. 2008) in the case  $\phi = \pi$  with  $f(\pi) = 1$  where adhesion, bending rigidity and thickness were varied. It should be noted however that the folds were observed to include some plastic deformation and the measured angles  $\theta$  were half the predicted ones. A

good agreement was also observed in the case  $\phi \ll 1$ , where  $f(\phi) \sim \phi/4$  and the triangle angle did vary linearly with the peeling angle (Kruglova et al. 2011). In this last article the “elastic” converging effect was put in competition with the geometric divergence of the cracks when peeling on a curved substrate.

In the limit of vanishing bending rigidity  $B \rightarrow 0$ , we see that the  $\sin \theta \sim \sqrt{l} \sim B^{1/6}$  also vanishes and we recover the  $\theta = 0$  prediction of our inextensible fabric model, although the convergence is rather slow. The attraction of the cracks towards each other is faster when the adhesion is high, and the accuracy of the inextensible fabric model will therefore depend on the strength of adhesion.

In general, with strong adhesion the converging effect is significant. This is particularly annoying when we try to remove adhesive tape and only manage to peel part of it (then the flap will always end up in a triangular shape). They are also observed on torn posters in public spaces, which are considered by artist Jacques Villeglé as a collective anonymous form of art (Duplaix 2008).

#### 4.1.1 Conclusion

In the inextensible fabric model, propagation should take place perpendicularly to the pulled fold. In fact the elastic energy stored in the fold leads to converging paths: by converging towards each other, the cracks reduce the width  $w$  of the fold and are able to release its energy.

### 4.2 Estimates for other cases

#### 4.2.1 Pulling on two cracks without adhesion

If adhesion is weak, or if the sheet is clamped on its boundaries without adhesion, the cracks are also observed to be attracted towards each other, and annihilate, leading to a pointy flap. A striking experimental result (Fig. 19) is that in the case of pulling on a sheet with clamped boundary condition with a pulling angle  $\phi = \pi$ , the shape of the resulting pointy flap is not a triangle, but follows a power law: the width of the flap  $w$  varies like the distance to the tip  $l$  like  $w \sim l^{3/4}$ . However a different exponent ( $w \sim l^{2/3}$ ) is observed in a “three flap” experiment (Bayart et al. 2011) as can be seen on Fig. 18. These configurations may seem at first similar (and indeed they are identical in the inextensible fabric limit), illustrating the fact that we are interested in fine features of the crack trajectory which now depends on the details of the loading configuration.

In the framework presented here, the prediction of the shape of the flaps requires the precise knowledge of the elastic energy of the system. It is tempting to suppose again

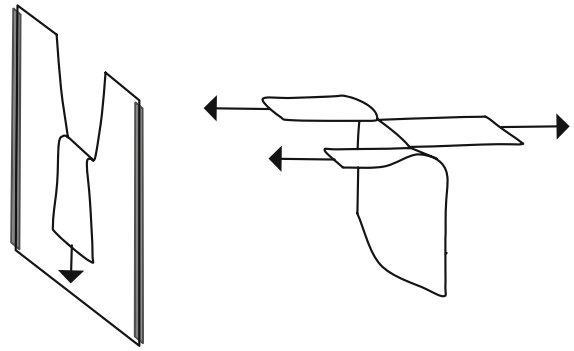


**Fig. 18** Different loading conditions lead to different converging exponents. Single flaps loading (left), and “three flaps” (right) experimental configurations were studied in Bayart et al. (2011)

that the elastic energy reduces to an energy localized in the fold, and therefore is a function of its width  $w$  and  $l - \delta$ ,  $E_{el}(w, l - \delta)$ . This is compatible with the fact that the crack path is very robust and does not seem to depend on its previous history. We therefore recover the equations seen before, with  $\Gamma = 0$  and  $\phi = \pi$ .

$$2F = 2G_c t \cos \theta$$

$$\left. \frac{\partial E_{el}}{\partial w} \right)_{(l-\delta)} = G_c t \sin \theta$$

The simplest estimate of  $E_{el}$  is to suppose that although adhesion is zero (and therefore does not dominate) the elastic energy can be estimated similarly through an elastica equation. In the limit of small angle  $\theta \ll 1$ , which is reasonable experimentally,  $F = G_c t$  and using Appendix 6.1,

$$\theta = 4 \sqrt{\frac{B}{w G_c t}} = 4 \sqrt{\frac{l_B}{w}} \tag{13}$$

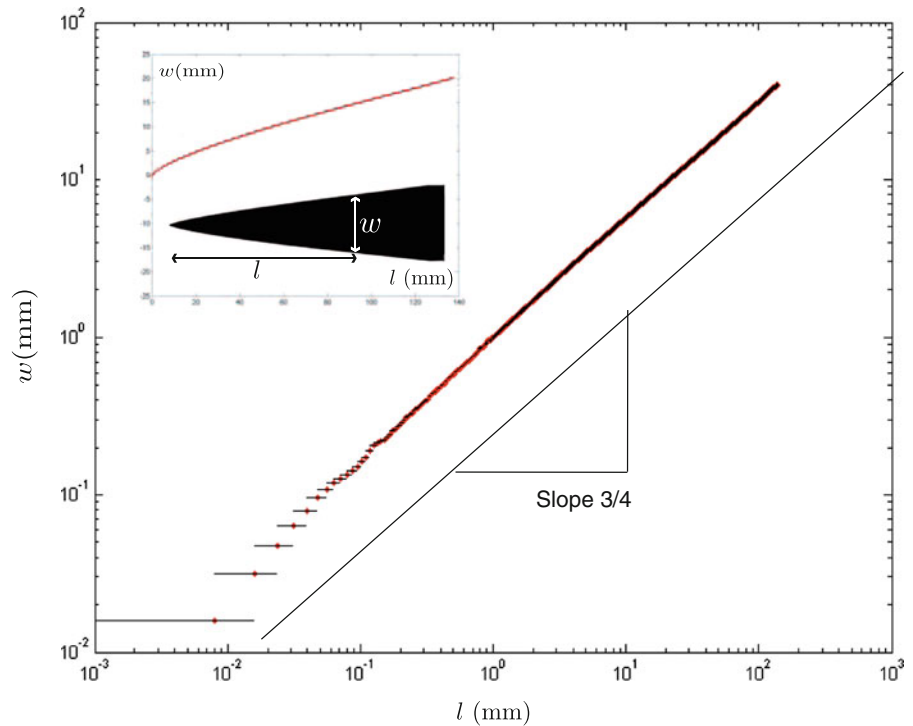
where we have defined

$$l_B = \frac{B}{G_c t}. \tag{14}$$

$l_B$  is a length which characterizes the magnitude of bending rigidity with respect to fracture property of a sheet. In experiments (Audoly et al. 2005; Bayart et al. 2011; Hamm et al. 2008; Roman et al. 2003),  $l_B$  was between 30 and 80  $\mu\text{m}$ , so that the predicted angles are indeed small. An interesting feature is that the converging angle increases when the cracks are closer together, as observed in the experiments (Fig. 19). However the predicted converging shape  $\theta \sim dw/dl$  leads to a power law of the type  $w \sim l_b^{1/3} l^{2/3}$ , with an exponent 2/3 close but different from the observed 3/4.

In fact the fold cannot be assumed to be a collection of identical elastica slices anymore. It may take a non

**Fig. 19** Experimental measurement of the shape of a torn flap: the width  $w \sim l^{3/4}$  follows a power law as function of distance to the tip  $l$  over at least 3 decades (the points at a distance  $l$  less than  $100 \mu\text{m}$  should might not be relevant, because  $l$  becomes comparable to the thickness of the sheet, even if they seem to align with the rest of the data). Inset: the same data in a linear plot. Data courtesy of V. Apablaza



develloppable shape, therefore including stretching energy as well as the bending energy considered before Witten (2007). In Bayart et al. (2011), the authors observe that the sheet is deformed on a large region ahead of the cracks, whose geometry gives an idea of stress distribution close to the crack tip. Although they lead to the correct exponent of the power law for two different loading configuration (one and three flaps), it is not clear yet how these geometrical arguments could be translated into the energy framework presented here. Note that this approach leads to predicted shape which are independent of mechanical properties ( $E$ ,  $G_c$ ) in contradiction with estimate (13). Another recent theoretical work based on the study of stress singularity (Cohen and Procaccia 2010) for non-linear plates, and a postulated generalization of the principle of local symmetry in this configuration predicts converging tears, but do not predict a power law shape.

#### 4.2.2 Pulling on one crack (pulled spiral)

In the case of the spiraling propagation of a single crack obtained when a flap is pulled (Fig. 8), the flap is deformed into a more complex shape (see Fig. 9), and are more difficult to describe. However we expect similar effect: bending energy involved in the fold can be released if the crack converges. Propagation should not take place

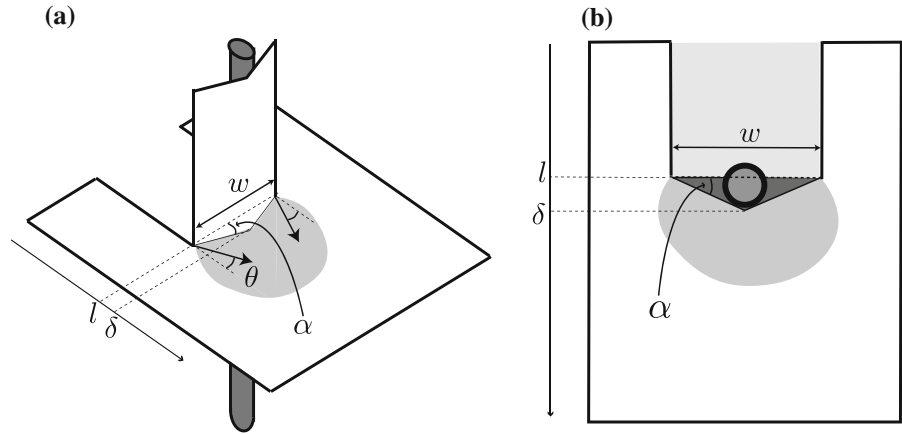
perpendicularly to the fold line (as the inextensible fabric model predicts) but slightly inwards.

In our experiments (Romero 2010; Romero et al. 2013), the radius of the spiral does grow exponentially  $r = r_0 \exp p\theta$  (with modulations which are due to the anisotropy of the material) as predicted by the inextensible fabric model. However the measured average exponential pitch is  $p = 0.24$ , a value close but significantly lower than  $p = 0.27$  expected from inextensible fabric theory. The fact that the growth factor of the spiral is lower than expected is due to the slight inward propagation. The propagation angle directly measured on the experiment is on average deflected inward by an angle on the order of  $3^\circ$ . This is close to the value of  $4^\circ$  predicted by Eq. (13) for a fold with  $w = 10\text{ cm}$ .

#### 4.2.3 Pushing on two cracks: diverging tears

We consider a sheet with two cracks, and a blunt tool pushed on the active front between the cracks. We have seen that if elastic energy is neglected, the propagation is perpendicular to the active front, and if one crack is blocked, an exponential spiral is observed. In fact in the experiment (Romero 2010; Romero et al. 2013), the pitch of the spiral is measured to be  $p = 0.29$ , larger than the theoretical prediction  $p = 0.27$ . This means that the direction of propagation is not perpendicular, but has a small

**Fig. 20** Elastic model for pushing on two cracks. **a** 3D view where the strained zone is presented in light gray. **b** Top view, where the indented triangular zone is colored in dark gray (compare with Fig. 22)



outwards component which is measured in the experiments as  $\theta \sim 2^\circ$  for a sheet with  $50\mu\text{m}$  thickness. Can this deviation from the inextensible fabric model be explained by including elastic energy?

We see on Fig. 20 that the force  $F$  results in an indentation of the front line, by a distance  $d = \delta - l$ , where  $l$  (resp.  $\delta$ ) corresponds to the position of the cracks (resp. of the pushing tool). It is reasonable to assume that the elastic energy is a function of the width  $w$  and of the indentation distance,  $E_{el} = E_{el}(w, l - \delta)$ .

The applied force  $F$  is computed by the formula  $Fd\delta = dE_{el}$  when the crack (and  $l$ ) is fixed (energy conservation), so that

$$F = \left. \frac{\partial E_{el}}{\partial \delta} \right)_{(l,w)} = - \left. \frac{\partial E_{el}}{\partial l} \right)_{(\delta,w)}$$

The second equality holds because  $E_{el}$  depends only on the relative position of the tool and the crack. If the crack propagates by a distance  $ds$  while the tool is held fixed ( $\delta = \text{cst}$ ), then Griffith's criterion

$$\left. \frac{\partial E_{el}}{\partial l} \right)_{(\delta,w)} dl + \left. \frac{\partial E_{el}}{\partial w} \right)_{(\delta,l)} dw + 2G_c t ds = 0$$

can be rewritten as

$$F \cos \theta + 2 \left. \frac{\partial E_{el}}{\partial w} \right)_{(\delta,l)} \sin \theta = 2G_c t$$

where we recognize a configuration similar to that of Eq. (8). We therefore obtain similar results:

$$F = 2G_c t \cos \theta \tag{15}$$

$$\left. \frac{\partial E_{el}}{\partial w} \right)_{(\delta,l)} = G_c t \sin \theta \tag{16}$$

Note that inward propagation ( $\theta > 0$ ) is predicted as before if the elastic energy increases with the distance between the crack.

Because an exact computation of the elastic energy  $E_{el}$  is difficult, we assume that it is entirely due to unavoidable stretching of the plate, which still bends infinitely easily. If the sheet is infinitely bendable, we can assume as in “tension field theory” (Davidovitch et al. 2011; Mansfield 1989; Stein and Hedgepeth 1961) that it cannot sustain compressive stresses, but only tensional stresses. The elastic response in this case is peculiar and non-linear. A simple estimate is to consider that an indentation distance  $d = l - \delta$  generates extensional strains on the order of  $(d/w)^2$ , on an area of size  $w^2$  (gray area in Fig. 20), so that the elastic energy would follow the scaling law  $E_{el} \sim Etw^2(d^4/w^4)$ . Similar arguments were used in Vermorel et al. (2010) to predict the number of cracks observed when an aluminum foil is perforated.

If we use this form of elastic energy

$$E_{el} = Et d^4 / w^2, \tag{17}$$

Equations (16) become for small angle  $\theta$ ,  $F = 4Et d^3 / w^2 = G_c t$ , so that (15) and (16) are the crack propagates in direction

$$\theta \simeq - \left( \frac{G_c}{E w} \right)^{1/3} = - \left( \frac{l_E}{w} \right)^{1/3} \tag{18}$$

when the angle of penetration  $\alpha = 2(\delta - l)/w$  reaches

$$\alpha_c \simeq \left( \frac{G_c}{E w} \right)^{1/3} = \left( \frac{l_E}{w} \right)^{1/3} \tag{19}$$

where we have defined

$$l_E = \frac{G_c}{E}$$

a material length which characterizes the fracture process.<sup>11</sup> In experiments (Audoly et al. 2005; Bayart et al. 2011; Hamm et al. 2008; Roman et al. 2003),  $l_E$  was

<sup>11</sup> It can be interpreted as a size around the crack tip where strains become large.

between 5 and 10  $\mu\text{m}$ , so that the predicted angles are again small.

Outward propagation ( $\theta < 0$ ) is indeed predicted because elastic energy decreases with the distance between the cracks  $w$ . The angle of propagation is here independent of the thickness of the sheet, but decreases with the width  $w$  of the active front. For the materials used in Romero (2010); Romero et al. (2013), this expression leads to angle on the order of  $3^\circ$  for  $w = 10\text{cm}$ , which has the right order of magnitude when compared to the divergence angle measured (Romero 2010; Romero et al. 2013) in the pushed exponential spiral (an average of  $2^\circ$ ).

Experimental measurements of the indentation force in geometries corresponding to that of Fig. 20 (but where the crack could not propagate Romero 2010) suggest the functional form

$$E_{el} = AEt w^2 (d/w)^n \tag{20}$$

for the elastic energy, where  $A$  is a dimensionless constant, confirming that stretching energy dominates in this system. However a surprising (and yet unexplained) fractional exponent  $n = 3.5$  was found instead of 4, leading to replacing the  $1/3$  exponent in equations (18) and (19) by  $1/(n - 1) = 0.4$ .

The diverging angle is therefore expected to depend weakly on the width  $w$  and tends to zero for large  $w$ . Using equation (17) in that limit, the shape of the diverging cut should be given by the differential equation  $dw/dl \sim -\theta \sim (l_E/w)^{1/3}$ , and a power-law shape

$$w \sim l^{3/4} l_E^{1/4} \tag{21}$$

Unfortunately, in experiments with brittle thin sheets, this diverging solutions is unstable and one of the crack dies, whereas the other one starts to oscillate as in Fig. 13. However when the experiment were performed on plastic material (metal sheets) (Wierzbicki et al. 1998), the instability is suppressed, and cracks are observed to diverge, together with an interesting pattern of plastic folds (see Fig. 21), which was named “concertina tearing” (Atkins 1995; Wierzbicki et al. 1998).

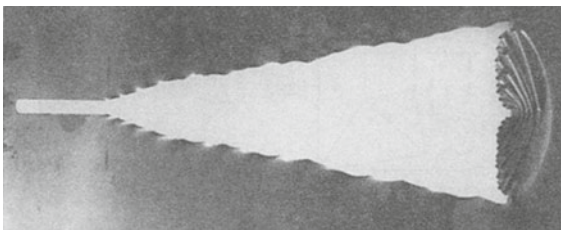


**Fig. 21** Concertina tear: diverging tears when a blunt object is pushing two cracks in a metal sheet, taken from Wierzbicki et al. (1998)

The transition between the oscillation and the concertina solution as plasticity increases is documented in a numerical study (Tallinen and Mahadevan 2011), but not yet really understood. Experiments in plastic materials (Wierzbicki et al. 1998) were initially motivated by the Exxon Valdez accident in 1989: the tanker’s hull was cut by a blunt rock, and because of the diverging path the resulting concertina opening was much bigger than the rock, causing a large oil spill and a major ecologic disaster. The wavelength is predicted through minimization of plastic dissipation to be  $\lambda \sim w^{2/3} t^{1/3}$ . The direction of propagation is estimated by the direction of maximum stress, leading to a power law  $w \sim t^{1/4} l^{3/4}$ , the same exponent  $l^{3/4}$  as in Eq. (21), but the crack path is here independent of material properties. It is surprising that although the cracks are diverging here, the global shape of the cut has the same geometry as the converging tears.

In experiments (Wierzbicki et al. 1998) and numerical simulations (Tallinen and Mahadevan 2011), the shape of the cut is compatible with such a power law. However the predicted independence on thickness or material parameter was not clearly tested (only one material tested, and one thickness), and the power law which gives a good fit of the torn shape was not tested on a large range of lengthscale. One may also wonder if the divergence in  $w \sim l^{0.71} l_E^{0.29}$  predicted by the rules (18) and (19) using the empirical energy (20) with  $n = 3.5$  could not also be compatible with the experimental data.

An explanation of the  $3/4$  exponent was recently given Tallinen and Mahadevan (2011), using the maximum energy release rate, completely neglecting plastic deformation. The wavelength  $\lambda \sim w^{2/3} t^{1/3}$  of the concertina is found as the minimum of elastic energy which is then estimated as  $E_{el} \sim B(w/t)^{1/3}$ . Using the equation  $G_c t \sin \theta = \partial E_{el} / \partial w$ , the authors conclude that the tears are diverging with an exponent  $3/4$ , but seem to forget the sign in the derivative. Because the elastic energy in this model increases with width  $w$ , the tears are in fact predicted to converge instead of diverging, which makes the model questionable.

#### 4.2.4 Pushing on one crack

We have noted that if the material behaves elastically, the diverging paths are not observed and instead only one crack remains, and oscillates (Fig. 10). In the inextensible fabric model, leaving aside the locking problem, these oscillations were found to be universal (tool independent) up to a scaling factor. How is the predicted crack path modified if we include elastic stretching energy?

We assume that the loading near the crack is similar to what it would experience in the double crack symmetric case studied above, and will propagate according to

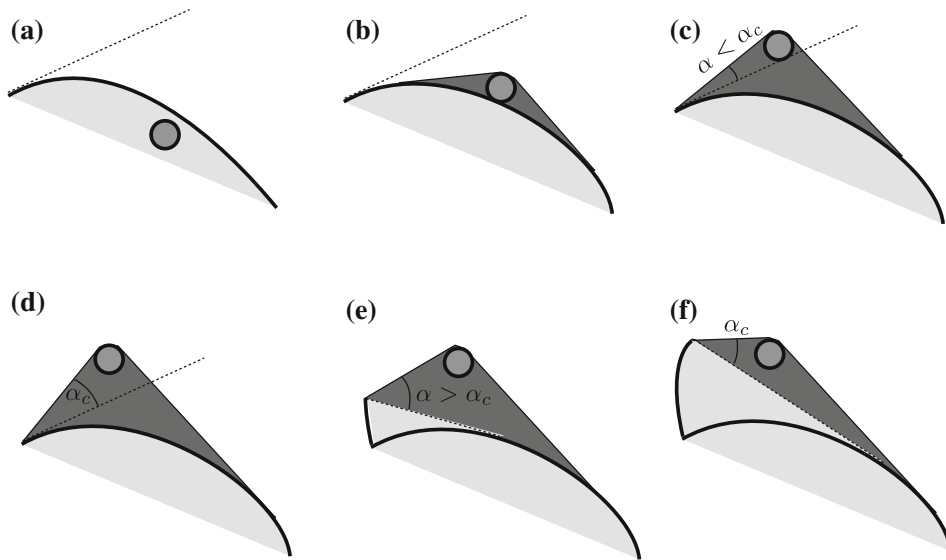


**Fig. 22** Unlocking propagation and dynamic phase: when the tool leaves the convex hull of the crack path (light gray area) by pushing on a non-active front (a–b), an indentation zone develops (dark gray) disconnected from the crack tip, in contrast with Fig. 20b. Propagation is possible only when indentation angle  $\alpha$

reaches the critical value  $\alpha_c$  (c, d). But as the crack advances, because of the curvature of the convex hull limit, the indentation angle increases (e), leading to a dynamic jump up to configuration (f) where  $\alpha = \alpha_c$  is recovered

the rules (18) and (19). These rules which take elasticity into account are still geometric at the end, and numerical integration lead to oscillations.

But a first remark is that the rules for propagation are not scale-invariant anymore, they depend on the size of the active front  $w$ . As a result, the crack path created by a large disk cannot be obtained through a simple zooming factor from the cut due to a smaller disk. In other words the wavelength  $\lambda$  and amplitude of the oscillations are not exactly proportional to the diameter of the object. However in practice the dependence on  $w$  is a weak power, and this non-linear dependence was not reported in experiments (Audoly et al. 2005; Ghatak and Mahadevan 2003; Roman et al. 2003). For the sake of simplicity, we will neglect this weak variation of the angle  $\theta$  with the object size so that the shape of the oscillation is independent of the shape of the object, and only depends on its width.

Another consequence is that the locking problem in the kinking event between each phase shift can now be solved by including elastic stretching. Before the kinking event (see Fig. 14b), the tool hits the curved crack path, but not the straight active front. Within the inextensible fabric model, the crack could not propagate and the tool was therefore locked. In cases where we push on a curved front, the rules (18, 19) were generalized (Audoly et al. 2005) in the following way: the difference of the convex hull of (crack path + tool) with the convex hull of the crack path alone (in light gray in Fig. 22) defines an indented

zone (in dark gray in Fig. 22). This indented zone plays the same role as the indented active front in Fig. 20b. But here this zone is not initially connected to the crack tip because of the curvature of the cut (see Fig. 22b). As the tool advances, the indented zone also grows, finally reaching the crack tip, and defining the effective indentation angle  $\alpha$  (Fig. 22c). When  $\alpha$  reaches the critical value computed at (19), propagation may take place, in direction  $\theta$  given by (18), with respect to the tangent to the crack. As the crack propagates, both convex hulls grow, but the indentation angle  $\alpha$  is found to increase instead of decreasing (Fig. 22e): the condition for propagation is overshoot, and a dynamic phase takes place. These dynamic jumps are clearly observed in the experiments (Audoly et al. 2005; Ghatak and Mahadevan 2003; Roman et al. 2003).

During these phases, the quasi-static approach is not relevant anymore, so that we must make an arbitrary assumption on the direction of propagation. A first option is to assume that the crack keeps a constant direction with respect to the active front of the crack convex hull. In that case we would recover the property that the path is independent of the shape of the tool (only depending on its width). In Audoly et al. (2005) the direction of propagation is assumed to follow a constant angle  $(\pi/2 - \theta - \alpha_c)$  with respect to the limit of the indented zone (18). This condition is equivalent to (18) when propagation is quasi-static, because (19) is satisfied. But because the evolution

of the indented zone depends on the details of the shape of the tool, a weak dependence of the crack trajectory on the shape of the tool is predicted, which can be fitted to that observed in experiments (Audoly et al. 2005).

#### 4.2.5 Instability of a straight crack path

The inextensible fabric model nicely describes the oscillating propagation of the crack, but another solution exists (at least when using a symmetric tool) where the crack propagates on a straight line ahead of the tool. This solution is never observed in experiments, and therefore must be unstable, so that the left-right symmetry of the problem is broken. Only if the tool has a width much smaller than the thickness of the film, the straight path is stable. The instability only develops when the tool becomes on the order of 4–5 times the thickness (Roman et al. 2003).

It is clear that the inextensible fabric model and the more refined description including stretching energy cannot predict the instability onset, because they don't include any thickness dependence. The nature of the instability can only be understood when bending and stretching effect are included. An experimental investigation of this instability was performed with an inclined tool (Reis et al. 2008), where stretching spreads on a larger zone, with the result of restabilizing the straight path if the tool is more inclined, even for a tool much wider than the sheet's thickness. The influence of material response was also investigated, as plasticity developing around the crack tip in experiments conducted at very slow speed favors straight propagation (Reis et al. 2008).

#### 4.2.6 Perforation experiments

When an object impacts on a clamped plate perpendicularly to its plane, a pattern of cracks may develop with a characteristic radial geometry. The understanding of this phenomenon requires the description of the interaction of bending and stretching waves with crack propagation (Vermorel et al. 2009; Villermaux and Vandenberghe 2013). In a quasistatic version (Vermorel et al. 2010), a cone is pushed perpendicularly through a plate, and the evolution of a pattern of radial cracks is observed. Here in most cases the symmetry imposes radial crack path propagation, and the question is really to predict the number of cracks. Assuming a number  $n$  of cracks, and using estimates of the elastic energy similar to Eq. (20), Griffith's criterion was applied to determine the equilibrium position of cracks, and therefore the total energy. The optimal number  $n$  which minimizes the total energy of the system is a function of  $G_c/Ew$ , where  $w$  is now the local radius of the cone. In the experiments, the value of this non-dimensional number is small, and in practice the optimal

number of crack is always close to 4, and hardly reaches 5 for large values of the non dimensional values of  $G_c/Ew$ .

It is interesting to compare this prediction with the inextensible fabric model, where elasticity is neglected. Geometry shows that for  $n$  radial cracks, the length of the cracks is just  $w/\cos(\pi/n)$  and the energy to minimize is simply the fracture energy  $G_c t w n / \cos(\pi/n)$  which has a minimum for  $n = 4$ . The inextensible fabric model therefore gives a good estimate of the optimal crack pattern.

However in experiments starting from a random distribution of cracks, the system evolves most of the time towards a radial crack pattern with 4–11 cracks, because of energy barriers preventing the evolution of the number of cracks towards the optimal number. The authors also report the observation of multiple spiraling branches (Vermorel 2010), which are certainly collaborative version of the pushed spirals reported in Romero (2010). It would be interesting to compare their pitch to predictions of the inextensible fabric model including multiple cracks.

#### 4.3 Conclusion on elastic effects

A complete understanding of tearing should include thin plate elasticity: bending and stretching effects should be included together with the geometrical non-linearities (the only ingredient in the inextensible fabric limit). But such a complete description is difficult from an analytical point of view, except in some isolated cases.

In the pushing case, stretching energy seems to dominate over bending energy, and deflects the cracks from the inextensible fabric model trajectory outwards by an angle  $\theta \sim (G_c/Ew)^{1/3}$ . This is because for a given indentation, the elastic energy decreases with inter-crack distance  $w$ , and therefore can be released when the cracks move away from each other. The inextensible fabric model predictions are valid when  $\theta \ll 1$  or equivalently when

$$F \sim G_c t \ll E t w$$

and we recover here the condition of (2) which ensures that stretching energy can be neglected. This condition can be rewritten

$$w \gg l_E = G_c/E \tag{22}$$

using the characteristic lengthscale  $l_E$ . Large systems compared to this lengthscale  $l_E$  can be considered almost inextensible.

In the case of tearing by pulling, the cracks (which are expected to propagate perpendicularly to the pulled fold in the inextensible fabric model) are deflected inwards by bending effects. Part of the bending energy of the fold can indeed be released when its size is reduced. The deflection angle is on the order of

$$\theta \sim \frac{B}{RG_{ct}} \sim \sqrt{\frac{BF}{w} \frac{1}{G_{ct}}}$$

where  $R$  is the typical radius of curvature of the fold, due to the applied force  $F$ .

In absence of adhesion, the typical force for tearing is on the order of  $F \sim G_{ct}$  and the deflection will be small ( $\theta \sim \sqrt{B/G_{ct}w} \ll 1$ ) when

$$F \sim G_{ct} \gg B/w$$

or equivalently when

$$w \gg l_B = \frac{B}{G_{ct}}. \tag{23}$$

Bending effects on the cracks path are negligible only if the system size is “large enough”,  $w \gg l_B$ , compared to the bending lengthscale  $l_B = B/G_{ct}$ .

We had written earlier (in Sect. 2) the necessary condition for which we expect the bending state of the sheet to be close to that of an inextensible fabric : the size  $R$  of the fold had to be small compared to the length of the flap (2) or  $F \gg Bw/L^2$ . This is equivalent to

$$L \gg \sqrt{wl_B}. \tag{24}$$

This condition ensures that curvature is localized in a small region (compared to the size of the system), a necessary hypothesis to apply our infinitely flexible model. We note that if both conditions are satisfied, then  $L \gg l_B$ . A necessary condition for the validity of the inextensible fabric is therefore that all dimensions ( $w, L$ ) of the system are large<sup>12</sup> compared to the bending length scale  $l_B$ . We note in particular that if the geometry of a system is scaled up (but keeping the thickness constant), all conditions (22–24) will be eventually satisfied, and in this sense inextensible fabric model applies to large systems.

In the case of strong adhesion  $\Gamma w \gg G_{ct}$ , the pulling force is  $F \sim w\Gamma$ , and the deviations to the inextensible fabric model are of the order of  $\sqrt{\Gamma B}/G_{ct}$ . We see that the magnitude of these deviations depend on the strength of adhesion, but not on the size  $w$  of the system. The inextensible fabric model is rarely a very good approximation in this case.

Apart from the case of peeling with strong adhesion, current theories are approximate at best, and only partial understanding is achieved, even in simple cases. We also lack a unified picture which would determine clearly which effect should be included in the theories: bending or stretching? or both?

<sup>12</sup> But condition (24) is more restrictive, the condition on the length of the flap depends on its width.

## 5 Conclusion

In this review we have seen in different experiments the remarkable features of quasistatic brittle tearing (fracture propagation in isotropic thin sheets when large out-of-plane bending is involved). Fracture paths are extremely reproducible, and follow regular geometric figures.

This is due to the fact that in a first approximation the sheets can often be considered as inextensible and infinitely flexible (the inextensible fabric model). In such simplified systems, there is no elasticity, and only the geometrical non-linearities are left, so that fracture mechanics obeys geometry. Although these configurations are highly non-linear, they might be an interesting example to teach in an introduction to fracture mechanics, because they convey essential non-trivial features of Griffith’s criterion without the mathematical difficulties of three-dimensional elasticity. We note that these geometrical rules are modified when the material is anisotropic (Takei et al. 2013), the crack path remaining highly reproducible, but depending on the variation of fracture energy  $G_c$  with orientation.

A better description of the system should include non-linear thin sheet elasticity, but this leads to great difficulties, and only one case is really accessible to the analysis. Nevertheless rough estimates suggest that the geometrical rules obtained in the inextensible fabric model should be a good guide for analysis *if the system is large compared to two lengthscales*:

$$l_E = G_c/E,$$

which characterizes the effect of membrane stresses and

$$l_B = B/G_{ct},$$

which quantifies the effect of bending stiffness,<sup>13</sup> where  $G_c$  is the fracture energy,  $E$  the Young’s modulus,  $B$  the bending rigidity, and  $t$  the thickness of the plate.

**Acknowledgments** I thank K. Ravichandar for his suggestions and comments. I also thank José Bico and Basile Audoly for invaluable help.

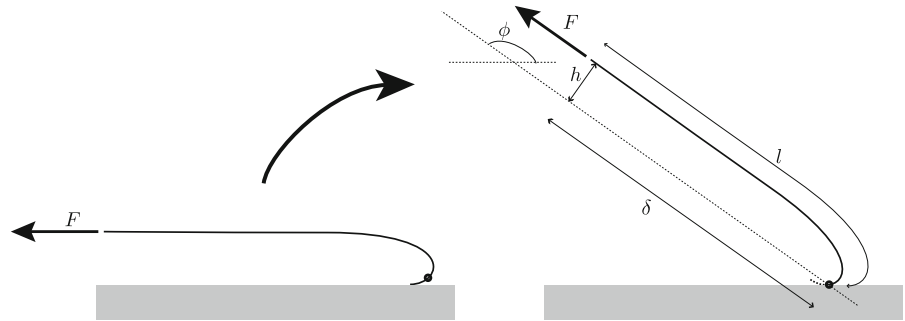
## 6 Appendix

### 6.1 Peeling an elastica

We consider an inextensible rod, with a tangent having an angle  $\theta$  at the point of curvilinear abscissa  $s$ , subject to a horizontal force  $F$  (see Fig. 23). The torque balance on an element with size  $ds$  reads  $dM/ds + F \sin \theta = 0$ , where

<sup>13</sup> An additional condition ensures that curvature in folds is localized on an area much smaller than the system size.

**Fig. 23** A portion of the shape of a peeled elastica with an angle  $\phi = \pi$  (left) leads to an angle  $\phi$  when rotated (right)



the constitutive relation  $M = Bd\theta/ds$  can be used. Here the bending rigidity is  $B = Et^3/12(1 - \nu^2)$ , where  $t$  is the thickness of the sheet,  $E$  its Young modulus, and  $\nu$  Poisson's ratio.

Finally, the elastica equation is Landau and Lifshitz (1967), Love (1944)

$$B\ddot{\theta} + \frac{F}{w} \sin \theta = 0$$

with the boundary conditions  $\theta(0) = 0$ , and a force  $F$ , but no torque applied at  $s = L$ ,  $\dot{\theta}(L) = 0$ . We can expect the flap to be curved only on a localized region near the clamped condition  $s = 0$ . What is the size of this region? Dimensional analysis directly shows that the only length-scale left in the problem is  $\sqrt{Bw/F}$ , so that the flap shapes for different loading and rigidity will all be similar, up to a simple scaling factor, as long as they are long compared to this radius of curvature,  $L \gg \sqrt{Bw/F}$ . The elastic energy per unit width which only depends on  $B$  and  $F/w$  can only be written as  $E_{el}/w = a\sqrt{FB/w}$ .

These results are also found by estimating the radius of curvature of the fold  $R$  from a torque balance. The torque  $Bw/R \sim FR$  is produced by force  $F$  with a lever arm of the order of  $R$ . Because  $1/R \sim \sqrt{F/Bw}$ , we also find that  $E_{el} \sim Bw/R \sim \sqrt{BFw}$ . We also note that the bending energy density scales like  $F/w$ .

In fact these quick arguments can be made exactly because an explicit solution is available in the case where  $L = \infty$ : we first normalize all distances by the typical length  $\sqrt{Bw/F}$  and find  $\dot{\theta} + \sin \theta = 0$ . Here we look for the solution where with the condition  $\theta(0) = 0$ ,  $\theta(\infty) = \pi$ ,  $\dot{\theta}(\infty) = 0$ . These solutions are the same as the 2D meniscus of a liquid under gravity and surface tension (Roman et al.).

A first integral of this equation gives  $\dot{\theta}^2/2 = 1 + \cos \theta$ , using the boundary conditions at  $s = \infty$ . If we keep  $\dot{\theta} > 0$ , this can be rewritten into  $\dot{\theta} = 2 \cos \theta/2$ , which can be integrated into

$$\sin(\theta/2) = \tanh(s).$$

This implicit solution with  $s \in [0, \infty]$  corresponds to a peeling angle  $\phi = \pi$ . But for a different peeling angle

$\phi$ , the solution is simply a rotated portion of the same solution  $s \in [s_0, \infty]$ , where  $\tanh(s_0) = \sin(\pi/2 - \phi/2) = \cos(\phi/2)$ , as seen in Fig. 23.

We compute the nondimensional elastic energy using these solutions:

$$E_{el}/\sqrt{FBw} = \int_{s_0}^{\infty} \dot{\theta}^2/2 ds = 2 \int_{s_0}^{\infty} \cos^2(\theta/2) ds = 2[\tanh(s)]_{s_0}^{\infty} = 2[1 - \cos(\phi/2)].$$

Finally we obtain

$$E_{el} = 2\sqrt{FBw}[1 - \cos(\phi/2)] \tag{25}$$

Another estimate gives in  $\int \dot{\theta}^2/2 ds = \int (1 + \cos \theta) ds = l - \delta$ , where  $l$  and  $\delta$  are the distances on Fig. 23. In dimensional terms, we find

$$E_{el} = F(l - \delta), \tag{26}$$

which shows that

$$l - \delta = 2\sqrt{Bw/F}[1 - \cos(\phi/2)] \tag{27}$$

and

$$E_{el} = \frac{4Bw}{(l - \delta)} [1 - \cos(\phi/2)]^2 \tag{28}$$

Yet another interesting quantity is based on direct integration, which shows that  $h = \int \sin \theta = -[\dot{\theta}]_{s_0}^{\infty} = 2 \cos(\theta(0)) = 2 \sin(\phi/2)$ . In dimensional form, this means that

$$h = 2\sqrt{Bw/F} \sin(\phi/2) = (l - \delta) \frac{\sin(\phi/2)}{1 - \cos(\phi/2)} \tag{29}$$

and to the elastic energy

$$E_{el} = \frac{4Bw}{h} [1 - \cos(\phi/2)] \sin(\phi/2) \tag{30}$$

### 6.2 Why does the crack loose memory (almost) instantaneously?

In the pulling configuration of pulling on an adhering sheet (Fig. 16), the past history of the crack only enters the

problem through the shape of the flap. We consider that the flap continues to have a cylindrical shape invariant in the  $z$  direction. The elastic energy reads

$$E_{el} = \frac{B}{2} \int_0^\infty w(u) \kappa^2(u) du$$

where  $u$  is the curvilinear abscissa along the fold, and the function  $\kappa(\cdot)$  is the curvature of the fold, an universal function that depends on  $(l - \delta)^{-1}$ . As the cracks propagate by  $\delta s$ , this energy varies for two reasons: the profile  $w(l)$  is modified because the origin of the fold has advanced by  $\delta l$ , and the curvature profile is modified (because  $l - \delta$  has changed).

$$\begin{aligned} \delta E_{el} &= \frac{B}{2} \int_0^\infty [w(u + \delta l) - w(u)] \kappa^2(u) du \\ &+ \frac{B}{2} \int_0^\infty w(u) \delta [\kappa^2(u)] du \end{aligned}$$

The key point is that the curvature profile is localized on a small region with size  $r$  comparable to  $l - \delta$ . If we assume that on this small lengthscale,  $w(u + \delta l) - w(u)$  can be replaced by  $\delta l (dw/du)_{u=0}$  and  $w(u) \sim w(0)$ , we get

$$\begin{aligned} \delta E_{el} &= \left. \frac{dw}{du} \right)_{u=0} \delta l \frac{B}{2} \int_0^\infty \kappa^2(u) du \\ &+ w(0) \frac{B}{2} \delta \left[ \int_0^\infty \kappa^2(u) du \right] \end{aligned}$$

In the first term we recognize the elastic energy of a slice of fold with unit width, multiplied by the the variation  $\delta w$ . Because of the invariance of the fold in direction  $z$ , this is exactly

$$dw \left. \frac{\partial E_{el}}{\partial w} \right)_{(l-\delta)}$$

whereas the second term is in fact a derivative where the width  $w = w(0)$  is held constant:

$$\left. \frac{\partial E_{el}}{\partial (l - \delta)} \right)_w d(l - \delta)$$

so that we recover the equations of Sect. 4.1

$$dE_{el} = \left. \frac{\partial E_{el}}{\partial (l - \delta)} \right)_w d(l - \delta) + dw \left. \frac{\partial E_{el}}{\partial w} \right)_{(l-\delta)}$$

When inserted in Griffith's criterion, all the quantities depend on  $w$  and  $dw/ds$ , so that finally the equation of evolution of the width can only be a first order equation of the type  $dw/ds = \mathcal{F}(w)$ : the evolution of the inter-crack distance  $w$  only depends on its actual value, not on the past.

References

Adda-Bedia M, Amar M (1996) Stability of quasi-equilibrium cracks under uniaxial loading. *Phys Rev Lett* 76(1996):1497–1500

Amestoy M, Leblond JB (1992) Crack paths in plane situationii, detailed form of the expansion of the stress intensity factors. *Int J Solids Struct* 29(4):465501

Argon A (1959) Surface cracks on glass. *Proc R Soc A* 250:472

Atkins A (1995) Opposite paths in the tearing of sheet materials. *Endeavour* 19(1):2–10

Atkins A (2007) Wiggly crack paths in the tearing of thin films. *Eng Fract Mech* 74:1018–1025. doi:10.1016/j.engfracmech.2006.12.006

Audoly B, Pomeau Y (2010) Elasticity and geometry: from hair curls to the non-linear response of shells. OUP, Oxford

Audoly B, Reis PM, Roman B (2005) Cracks in thin sheets: when geometry rules the fracture path. *Phys Rev Lett* 95(025):502 doi:10.1103/PhysRevLett.95.025502

Bayart E, Boudaoud A, Adda-Bedia M (2010) On the tearing of thin sheets. *Eng Fract Mech* 77:18491856. doi:10.1016/j.engfracmech.2010.03.006

Bayart E, Boudaoud A, Adda-Bedia M (2011) Finite-distance singularities in the tearing of thin sheets. *Phys Rev Lett* 106(194):301. doi:10.1103/PhysRevLett.106.194301

Ben-Amar M, Pomeau Y (1997) Crumpled paper. *Proc Math* 453:729–755

Bico J, Roman B, Moulin L, Boudaoud A (2004) Elastocapillary coalescence in wet hair. *Nature* 432(7018):690–690. doi:10.1038/432690a

Bourdin B, Francfort G, Marigo JJ (2008) The variational approach to fracture. *J Elast* 91:5–148. doi:10.1007/s10659-007-9107-3

Bui H (1978) Mécanique de la rupture fragile. Masson, Paris

Cerda E, Hamm L, Roman B, Romero V (2012) Film mince d'emballage amorce de dchirure. INPI (2953499)

Cerup-Simonsen B, Tornqvist R, Lutzen M (2009) A simplified grounding damage prediction method and its application in modern damage stability requirements. *Marine Struct* 22: 62–83

Chambolle A, Francfort G, Marigo JJ (2009) When and how do cracks propagate? *J Mech Phys Solids* 57:16141622

Cohen Y, Procaccia I (2010) Dynamics of cracks in torn thin sheets. *Phys Rev E* 81:066103. doi:10.1103/PhysRevE.81.066103

Cotterell B, Rice J (1980) Slightly curved or kinked cracks. *Int J Fract* 16(2):155169

Davidovitch B, Schroll RD, Vella D, Adda-Bedia M, Cerda EA (2011) Prototypical model for tensional wrinkling in thin sheets. *Proc Natl Acad Sci USA* 108(45):18227–18232. doi:10.1073/pnas.1108553108

Dillard D, Hinkley J, Johnson W, St. Clair T (1994) Spiral tunneling cracks induced by environmental stress cracking in larc-tpi. *J Adhesion* 44: 1–2, 51–67. doi:10.1080/00218469408026616

Duplaix S (2008) Jacques Villéglé, la comdie urbaine. Centre Georges Pompidou Service Commercial

Eiffel G (1900) La Tour de Trois Cent Metres. Société des Imprimeries Le Mercier, Paris

- Ghatak A, Mahadevan L (2003) Crack street: the cycloidal wake of a cylinder tearing through a thin sheet. *Phys Rev Lett* 91:215507
- Gladden J, Belmonte A (2007) Motion of a viscoelastic micellar fluid around a cylinder: flow and fracture. *Phys Rev Lett* 98(223):501. doi:10.1103/PhysRevLett.98.224501
- Goldstein R, Salganik R (1974) Brittle fracture of solids with arbitrary cracks. *Int J Fract* 10(2):507523
- Hakim V, Karma A (2009) Laws of crack motion and phase-field models of fracture. *J Mech Phys Sol* 57(235501):342368
- Hamm E, Reis P, Leblanc M, Roman B, Cerda E (2008) Tearing as a test for mechanical characterization of thin adhesive films. *Nat Mater* 7:386–390. doi:10.1038/nmat2161
- Hui C-Y, Zehnder AT, Potdar YK (1998) Williams meets von Karman: Mode coupling and nonlinearity in the fracture of thin plates *International Journal of Fracture* 93:409–429
- Kendall K (1971) The adhesion and surface energy of elastic solids. *J Phys D Appl Phys* 4:1186–1195
- Kendall K (1975) Thin-film peeling- the elastic term. *J Phys D Appl Phys* 8:115
- Kruglova O, Brau F, Villers D, Damman P (2011) How geometry controls the tearing of adhesive thin films on curved surfaces. *Phys Rev Lett* 107(164):303. doi:10.1103/PhysRevLett.107.164303
- Landau L, Lifshitz E (1967) *Theory of elasticity*. Mir
- Lawn B (1993) *Fracture of brittle solids*. Cambridge University Press, Cambridge
- Lebental M (2007) *Chaos quantique et micro-lasers organiques*. Ph.D. Thesis, Univ Paris XI. <http://tel.archives-ouvertes.fr/tel-00194350>
- Leblond J (2003) *Mécanique de la rupture fragile et ductile*. Hermes Science Publications
- Leung KT, Jozsa L, Ravasz M, Nda Z (2001) Spiral cracks without twisting. *Nature* 410(6825):166. doi:10.1038/35065517
- Lobkovsky AE, Gentges S, Li H, Morse D, Witten TA (1995) Scaling properties of stretching ridges in a crumpled elastic sheet. *Science* 270:1482–1485
- Love A (1944) *Treatise on the mathematical theory of elasticity*. Dover, New York
- Mansfield EH (1989) *The bending and stretching of plates*. Cambridge university press, Cambridge
- Marigo JJ, Meunier N (2006) Hierarchy of one-dimensional models in nonlinear elasticity. *J Elast* 83:1–28. doi:10.1007/s10659-005-9036-y
- Meyer DC, Leisegang T, Levin A, Paufler P, Volinsky A (2004) Tensile crack patterns in mo/si multilayers on si substrates under high-temperature bending. *Appl Phys A* 78:303–305. doi:10.1007/s00339-003-2340-0
- Monsalve A, Gutierrez I (2000) Application of a modified rigid plastic model to the out-plane fracture of 'easy open end cans'. *Int J Fract* 102:323–339. doi:10.1023/A:1007625512996
- Néda Z, Leung K, Józsa L, Ravasz M (2002) Spiral cracks in drying precipitates. *Phys Rev Lett* 88(9):095502. doi:10.1103/PhysRevLett.88.095502
- O'keefe R (1994) Modeling the tearing of paper. *Am J Phys* 62(4):299–305. doi:10.1119/1.17570
- Pogorelov A (1988) *Bendings of surfaces and stability of shells*. American Mathematical Society, Providence
- Reis P, Kumar A, Shattuck MD, Roman B (2008) Unzip instabilities: straight to oscillatory transitions in the cutting of thin polymer sheets. *Eur Phys Lett* 82(64):002. doi:10.1209/0295-5075/82/64002
- Roman B, Bico J (2010) Elasto-capillarity: deforming an elastic structure with a liquid droplet. *J Phys-Condens Mater* 22(49). doi:10.1088/0953-8984/22/49/493101
- Roman B, Gay C, Clanet C (2013) Pendulum, drops and rods: a physical analogy. *Am J Phys* (submitted)
- Roman B, Reis PM, Audoly B, De Villiers S, Vigui V, Vallet D (2003) Oscillatory fracture paths in thin elastic sheets/oscillatory fracture paths in thin elastic sheets. *C R Mecanique* 331:811–816. doi:10.1016/j.crme.2003.10.002
- Romero V (2010) *Spiraling cracks in thin sheets*. Ph.D. Thesis, UPMC/USACH. <http://pastel.archives-ouvertes.fr/pastel-00552045>
- Romero V, Hamm E, Cerda E (2013) Spiral tearing of thin films. *Soft Matter* (in press). doi:10.1039/c3sm50564b
- Ronsin O, Heslot F, Perrin B (1995) Experimental study of quasistatic brittle crack propagation. *Phys Rev Lett* 75(12):2352–2355. doi:10.1103/PhysRevLett.75.2352
- Sendova M, Willis K (2003) Spiral and curved periodic crack patterns in sol-gel films. *Appl Phys A Mater Sci Process* 76:957–959. doi:10.1007/s00339-002-1757-1
- Stein M, Hedgepeth J (1961) *Analysis of partly wrinkled membranes*. Tech. rep, NASA, Langley research center, Langley Field, VA
- Struik D (1988) *Lectures on classical differential geometry*. Dover, New York
- Takei A, Roman B, Bico J, Hamm E, Melo F (2013) Forbidden directions for the fracture of thin anisotropic sheets: an analogy with the wulff plot. *Phys Rev Lett* 110(144):301. doi:10.1103/PhysRevLett.110.144301
- Tallinen T, Mahadevan L (2011) Forced tearing of ductile and brittle thin sheets. *Phys Rev Lett* 107(245):502. doi:10.1103/PhysRevLett.107.245502
- Timoshenko S, Woinowski-Krieger S (1959) *Theory of plates and shells*. McGraw-Hill, New York
- Vella D, Wettlaufer JS (2007) Finger rafting: a generic instability of floating elastic sheets. *Phys Rev Lett*. doi:10.1103/PhysRevLett.98.088303
- Vermorel R (2010) *Elasticité et fragmentation solide*. Ph.D. Thesis, Univ. Provence Aix-Marseille. PRL 104:175502. doi:10.1103/PhysRevLett.104.175502
- Vermorel R, Vandenbergh N, Villermaux E (2009) Impacts on thin elastic sheets. *Proc R Soc Lond A* 465:823842
- Vermorel R, Vandenbergh N, Villermaux E (2010) Radial cracks in perforated thin sheets. *Phys Rev Lett* 104
- Villermaux E, Vandenbergh N (2013) Geometry and fragmentation of soft brittle impacted bodies. *Soft Matter* (in press). doi:10.1039/C3SM50789K
- Wan N, Xu J, Lin T, Xu L, Chen K (2009) Observation and model of highly ordered wavy cracks due to coupling of in-plane stress and interface debonding in silica thin films. *Phys Rev B*. doi:10.1103/PhysRevB.80.014121
- Wierzbicki T, Trauth KA, Atkins AG (1998) On diverging concertina tearing. *J Appl Mech* 65:990
- Williams M (1961) The bending stress distribution at the base of a stationary crack. *J Appl Mech* 28:7882
- Witten TA (2007) Stress focusing in elastic sheets. *Rev Mod Phys* 79(2):643–675. doi:10.1103/RevModPhys.79.643

- Xiaa C, Hutchinson JW (2000) Crack patterns in thin films. *J Mech Phys Solids* 48:1107–1131
- Yang B, Ravi-Chandar K (2001) Crack path instabilities in a quenched glass plate. *J Mech Phys Solids* 49(2001):91–130
- Yuse A, Sano M (1993) Transition between crack patterns in quenched glass plates. *Nature* 362:329
- Zehnder AT, Viz MJ (2005) Fracture mechanics of thin plates and shells under combined membrane, bending, and twisting loads. *Appl Mech Rev* 58(1):37